

行政院國家科學委員會專題研究計畫 成果報告

自由空間奈米光機電技術

計畫類別：個別型計畫

計畫編號：NSC94-2215-E-009-028-

執行期間：94年01月01日至94年07月31日

執行單位：國立交通大學光電工程學系(所)

計畫主持人：田仲豪

計畫參與人員：洪健翔、簡銘進

報告類型：精簡報告

處理方式：本計畫可公開查詢

中 華 民 國 94 年 9 月 22 日

行政院國家科學委員會補助專題研究計畫 成果報告
 期中進度報告

自由空間奈米光機電技術

計畫類別： 個別型計畫 整合型計畫

計畫編號：NSC 94-2215-E-009-028-

執行期間： 94 年 1 月 1 日至 94 年 7 月 31 日

計畫主持人：田仲豪

共同主持人：

計畫參與人員：洪健翔、簡銘進

成果報告類型(依經費核定清單規定繳交)： 精簡報告 完整報告

執行單位：國立交通大學 光電工程學系

中華民國 94 年 9 月 20 日

自由空間奈米光機電技術

中文摘要

本次計畫中，我們在微機電平台上製作了具有一階分光功能之直立式微光柵及極化分光器，量測結果與計算結果誤差均在可預測範圍內。此光學微機電製程複雜，誤差來源主要來自製造上的差異性。我們成功嘗試以自動組裝技術減少製造上所產生的製程誤差，並探討光學在不同結構上的效應。

關鍵詞: 微光柵、極化分光器、微機電

Free space optical NEMS (nano-electro-mechanical systems) technology

Abstract

In this project, we study the design, fabrication and measurement of an out-of-plane grating and polarizer in the dimension of micrometers. Both devices have been demonstrated by the surface micromachining process. In order to reduce the fabrication error, we developed a process for self-assembly by means of surface tension of photoresist. Finally, the optical properties of various optical features have been discussed.

目錄

- 一、前言
 - 二、自由空間微光學元件基本原理
 - 三、微型極化分光器及微型光柵的建立與分析
 - 四、微光柵及微極化分光器的製程與量測結果
 - 五、未來研究方向與目標
 - 六、結論
 - 七、計畫成果自評
 - 八、參考文獻
- 附錄

一、前言

微光柵及微極化分光器為微光機電系統所常用的微元件。光柵主要應用於分光，而極化分光器主要用於將兩不同極化方向之入射光以一定比率分開。以光儲存產業中的光學讀寫頭為例：其使用的三光束循軌法是將光柵置於雷射光出口處，使入射光繞射成 0 與 +/-1 階等三光束，其中零級繞射光束用來偵測聚焦與光碟片的資料讀取，而 +/-1 階光束用來偵測光碟片的軌道位置；而微極化分光器使用於系統中段，入射光從雷射出射被偏光片調變成單一極化方向（p 極化方向）可完全穿透極化分光器，至碟片反射並經過兩次四分之一相位延遲片最後剩另一單一極化方向（s 極化方向）回到極化分光器，極化分光器可將從碟片回來的光束反射至偵測器。

近年來由於微機電技術的進展，傳統的光學讀寫頭改以微機電製作的方法紛紛被提出，其中以 M.C.Wu 等人所提到用 Pister[1]所提出微絞鏈技術組裝出自由空間型的微光學讀寫頭[2]的三維微光學桌最受矚目，主要原因在於其將主動及被動光學元件整合在一起，不過因系統過為複雜，以多晶矽構成的光學元件光學效率低，且組裝技術複雜。本計畫針對上述缺點提供可行之解決方案，利用 MUMPs-like[3]技術，設計製作出微光柵及微極化分光器，並進一步以此技術製作具極化分光功能之自由空間次波長光柵。

二、自由空間微極化分光器及微光柵的原理

2-1 基本光柵理論

所謂的光柵是在基本材料上製出週期性、連續性的狹長切口，最基本的形式為穿透式繞射光柵，如 Fig. 2-1 所示。此圖的左側有一平行入射平行光波前，與光柵的平面夾角為 α ，稱為入射角；而右側繞射光與光柵平面的夾角為 β ，稱為繞射角，而 a 為光柵一週期的長度。以最簡單的光路分析可得到光程差 $\Delta = \Delta_1 + \Delta_2 = a(\sin\alpha + \sin\beta)$ 。

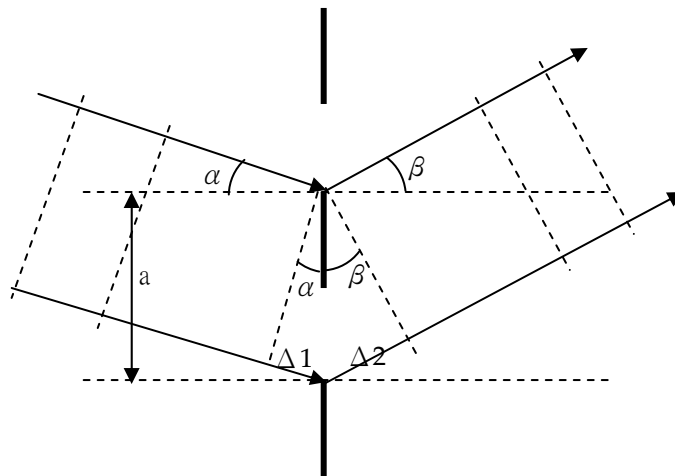


Fig. 2-1 穿透式繞射光柵

光程差包含兩個可能是相加或相減的正弦項，以繞射角 β 來決定。若入射光與繞射光的方向都在光柵正交面的同一側，則繞射角 β 為正，如圖所示；若入射光與繞射光方向在光柵證交面的異側，則繞射角 β 為負。當光成差之值與光波長的整數倍相等時，所有的繞射波就會有能量集中的現象發生，而繞射方程式即：

$$\Delta = \Delta_1 + \Delta_2 = a(\sin\alpha + \sin\beta) = m\lambda$$

其中 $m=0,+/-1,+/-2$

上式中的 m 為光柵繞射階數，當光柵繞射階為零時，不論入射光波長的大小為何，均可由上式得到的 $\beta = -\alpha$ 關係。此一關係的意義為入射光通過光柵之後並不會偏折一角度，亦即入射光與繞射光將沿一直線方向進行。若入射光 α 為一定值，在固定繞射階數下，繞射角 β 隨著波長而改變，即不同光的繞射角會不同。

2-2 基本極化分光器理論

所謂極化分光器是使自由空間傳波之光束通過折射率不同之媒體介面，造成光束的折射與反射，加上光學布魯斯特角的原理可造成極化分光。其最基本的形式是單一層薄膜，如 Fig. 2-2 所示，當一束光遇到兩種折射率不同的媒體界面時，一般來說部份反射部分折射。為說明反射和折射佔多少比例，通常引入反射率和透射率的觀念，此處 p 分量和 s 分量要分別計算，考慮振幅反射率：

$$r_p = \frac{E'_{1p}}{E_{1p}} = \frac{n_2 \cos i_1 - n_1 \cos i_2}{n_2 \cos i_1 + n_1 \cos i_2}$$

$$r_s = \frac{E'_{1s}}{E_{1s}} = \frac{n_1 \cos i_1 - n_2 \cos i_2}{n_1 \cos i_1 + n_2 \cos i_2}$$

$$t_p = \frac{E_{2p}}{E_{1p}} = \frac{2n_1 \cos i_1}{n_2 \cos i_1 + n_1 \cos i_2}$$

$$t_s = \frac{E_{2s}}{E_{1s}} = \frac{2n_1 \cos i_1}{n_1 \cos i_1 + n_2 \cos i_2}$$

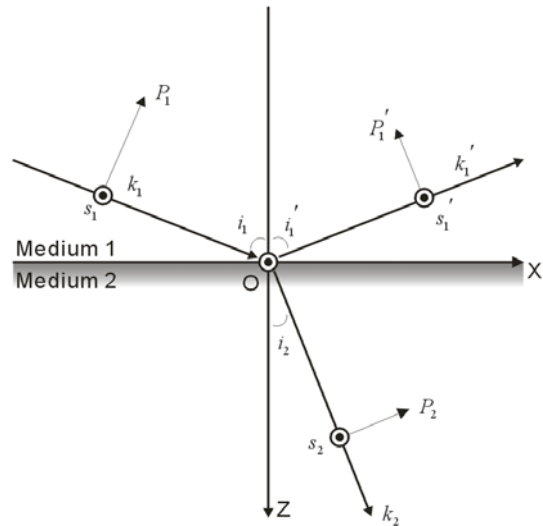


Fig. 2-2 光斜向入射不同介質

上式 r_p 、 r_s 分別為 p 分量及 s 分量的反射率； t_p 、 t_s 分別為 p 分量和 s 分量的穿透率，由 r_p 運算式及折射定律 $n_1 \sin i_1 = n_2 \sin i_2$ 可得到布魯斯特角的運算式。當入射光以布魯斯特角 (Brewster's angle) 入射時 r_p 值為零，此情況下 p 分量光束會完全穿透。傳統極化分光器基本結構為單層或多層薄膜（一般為氮化矽或二氧化矽），工作在入射光以布魯斯特角入射薄膜

的狀態下，此時光束 p 分量會完全穿透，而 s 分量 70%~100%被薄膜反射至另一方向達到極化分光的效果。一般增加薄膜數目以不同材料交互堆疊可增加 s 分量的總反射比率。

2-3 次波長光柵理論

傳統作為偏極化用途之元件，主要包含雙折射晶體、二色性材料、材料之布魯司特角及金屬相位光柵等。自然界中有許多晶體，諸如方解石、石英、電氣石、雲母和冰等都具有雙折射的特性，它會使得同一束光中不同電場方向（極化）的光波於其內產生相位與折射角等差異，因此達到偏極化之用途。二色性材料主要利用材料本身對於某一個軸向之極化光產生吸收，而讓另一個軸向之極化光通過，一般偏光片即利用此種原理。而利用材料之布魯司特角雖亦可達到偏極化之效果，但由於受到特定入射角度的影響，大大限制了它的應用。而金屬相位光柵（wire-grid polarizer）是一種典型的光學元件，已廣泛的應用在無線電(radio-frequency)及紅外光(infrared region)的波段中。過去受到傳統製程技術的限制，波長較短的可見光並無法使用此種偏振元件。然而如今已有多項先進之製程技術(如e-beam lithography)可大幅改進微影時之線寬尺度(<100nm)，進一步縮小光柵的週期，製作出光柵週期在可見光波長以下的繞射光柵，稱為次波長繞射光柵(SOE)。利用光柵所製成的極化元件依照其功能可分為三種類型：(1) 極化分光片(Polarization beam splitter) (2) 極化相位延遲片(Polarization retardation element) (3) 極化旋轉片(Polarization rotator)，其功能如 Fig. 2-3 所示。

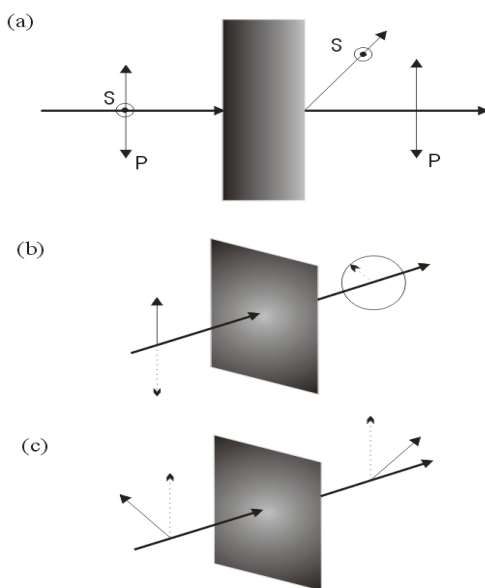


Fig. 2-3

不同類型之偏振元件功能

(a) 極化分光片

(b) 極化相位延遲片

(c) 極化旋轉片

然而光柵在不同的入射光波長時，其行為可分為三類：(1)當光柵之週期(Λ)遠大於入射光之波長($\Lambda \gg \lambda$) (2)光柵之週期(Λ)遠小於入射光之波長($\Lambda \ll \lambda$) (3) 光柵之週期(Λ)近似於入射光之波長($\Lambda \approx \lambda$)。第一種光柵與入射光的極化方向幾乎沒有關連性，因此此種光柵的行為光學僅採用純量理論(scalar regime)來解釋即可。而第二種光柵則是當光柵的週期小於入射波長的一半時($\Lambda < 0.5\lambda$)只剩下穿透光與零階的繞射光可以從此種光柵基板傳遞出來(含穿透光與反射光)，此種光柵亦稱之為零階光柵(zero order grating)。此種光柵需採用電磁波的嚴格繞射理論(rigorous diffraction theory)來解析極化光的情形，在某些簡化情形下亦可以

採用等效介質理論(effective medium theory)來分析。第三種光柵會是發生在光柵週期介於 5λ 至 0.5λ 之間($0.5\lambda < \Lambda < 5\lambda$)，會產生數階的繞射光，這些繞射光的效率與極化情形會隨著入射光的極化不同而改變。由於僅有少數幾階繞射光存在，所以此種光柵適合應用在需要高繞射效率光學系統中。

依據前段所述，當次波長光柵之寬度遠小於波長時，所有通過光柵之光將為零階繞射，然而因其光柵之材料與排列方式會影響光波於向量表現上之差異，故可以進一步將之簡化並等效為一層具有雙折射特性之材料 (Fig. 2-4)。以一維的次波長光柵為例，若光柵之材料折射率為 n_1 ，將其置於折射率為 n_2 之環境中，利用等效介質理論，我們可以將其雙折射特性描述為：

$$n_{TE} = \sqrt{fn_1^2 + (1-f)n_2^2}$$

$$n_{TM} = \frac{1}{\sqrt{fn_1^{-2} + (1-f)n_2^{-2}}}$$

其中 f 定義為光柵寬度 w 與週期 p 之比值，即 w/p ；TE為電場垂直入射面（紙面）方向；TM 則為電場平行入射面方向。依據式中的雙折射率，即可推算不同極化方向的光在通過該光柵時，所表現之穿透或反射效應。

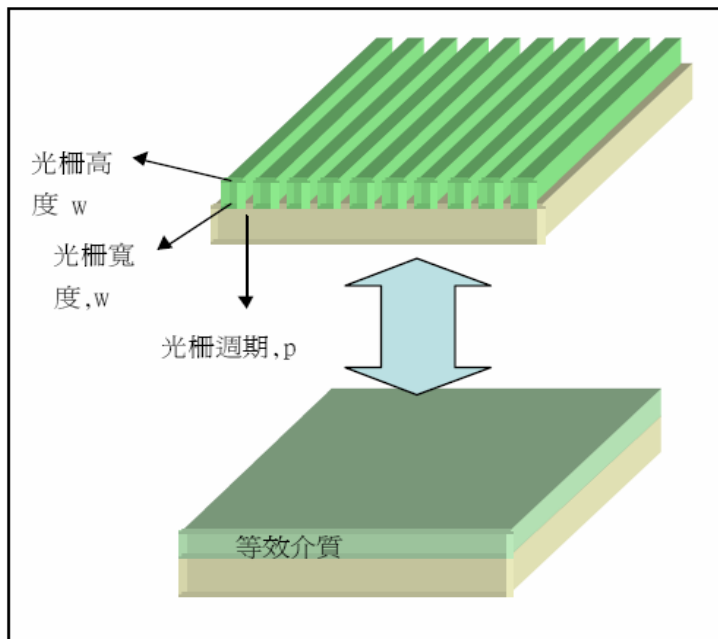


Fig. 2-4 次波長繞射光光柵等效介質示意圖

在採用嚴格繞射理論來分析光波的特性時，需探討光柵表面之入射行為。Fig. 2-5為一般表面輪廓(surface-relief)光柵之繞射幾何圖形，可以用下列參數來描述光柵的繞射問題(1)光柵深度(d) (2)光柵週期循環週期(D) (3)入射介質之折射係數(n_1) (4)光柵區域1之折射係數(n_{1g}) (5)光柵區域2之折射係數(n_{2g}) (6)基板介質之折射係數(n_2) (7)入射光與光柵法線之夾度(θ_i) (8)入射光與光柵面之夾角(φ_i) (9)入射光極化強度比例夾角(α_i) (10)入射光極化相位差角度 δ_i (11)光柵線寬(c)，因此我們可定義s極化分量為垂直入射平面之電場分量，而p極化分量為垂直入射平面之電場分量。藉由複雜之公式推導可得到光柵之週期：

三、 微型極化分光器及微型光柵的建立與分析

3-1 微光柵之建立與分析

3-1-1 繞射效率計算

首先我們需要訂出光柵的繞射效率進而計算出光柵的參數，光柵繞射效率的計算比繞射角複雜多了。目前有兩種方式：一為根據純量繞射理論，適用於光柵之週期大於入射光波長 10 倍以上時。另一為根據嚴格耦合波演算法 (Rigorous Coupled Wave Algorithm)，適用於任何尺寸的光柵週期，其計算較為複雜，目前已有商用軟體據此發展出，如 G-SOLVER。G-SOLVER 是相當容易學習的軟體，只需要輸入幾項參數就會自行計算各階的繞射效率，包括入射光波長、入射角、基材、外界環境的折射率、光柵厚度、階梯數及光柵的週期長度。

本計畫將以 G-SOLVER 計算出具有下列功能的穿透式微光柵所需的製程條件為：

1. 入射光波長 $\lambda=633\text{nm}$ 。
2. 入射角為零度 (平行入射光)。
3. 出射的繞射光角度：0 階與 ± 1 階夾角為 4 ± 0.5 度。
4. 出射的繞射光效率比：-1 階：0 階： $+1$ 階 $\cong 1:(4\sim 10):1$ 。
5. 光柵圖案由對 $\lambda=633\text{nm}$ 具穿透性的 SiN ($n=2.1$) 組成。

將上述條件帶入 G-SOLVER，我們可計算出光柵所需要的厚度計算出來，Fig.3-1 為厚度、Fill factor、繞射效率比(0^{th} order/ $\pm 1^{\text{st}}$ order)計算結果關係圖，虛線內為預設的範圍，製程可能造成的誤差已考慮在內。故我們欲製造厚度 $455\text{nm}\sim 480\text{nm}$ 可以以 LPCVD 控制之，若超過此值時，可使用熱磷酸將厚度降低。Fill factor 理想值 0.5，考慮到製程誤差範圍在 $0.4\sim 0.6$ 之間。

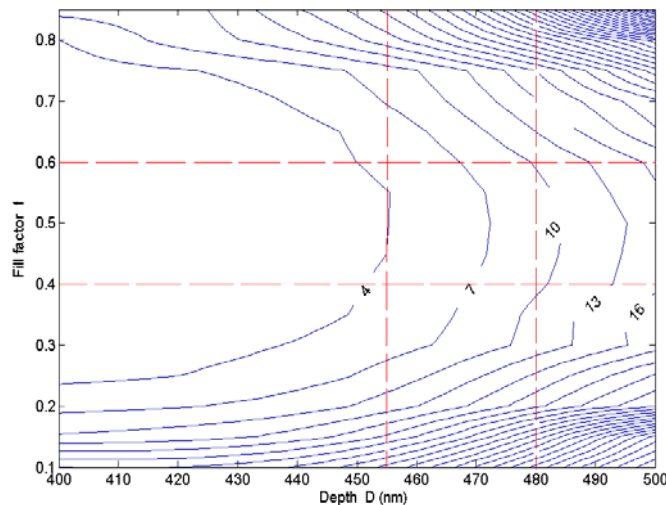


Fig. 3-1 厚度、Fill factor、繞射效率比的計算結果

3-1-2 輔助定位機構的設計

直立式微光柵的輔助定位機構設計包含了微樞紐及止動微結構兩部分。Fig. 3-2 為設計圖。

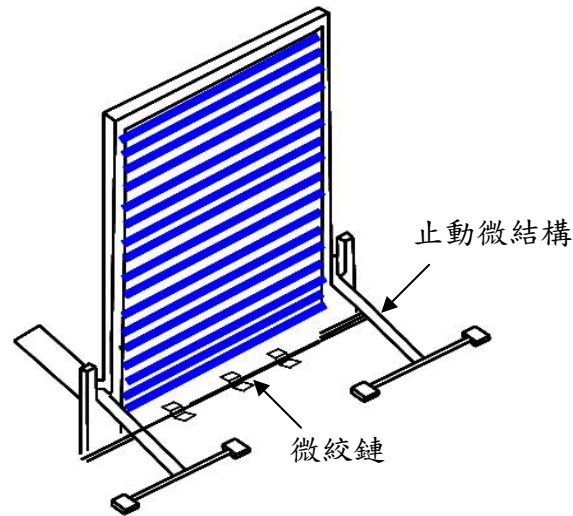


Fig. 3-2 微光柵設計圖

微絞鏈由 Pister[1]等四人所提出，經由微樞紐的結構設計使得利用面型微加工技術所製作的微元件在製作的微元件在結構釋放之後，可組裝成三度空間的微元件。如 Fig. 3-3 所示典型微絞鏈 SEM 圖。其結構皆可由多晶矽組成。兩層之間的空隙則由二氧化矽組成的犧牲層蝕刻而成的。

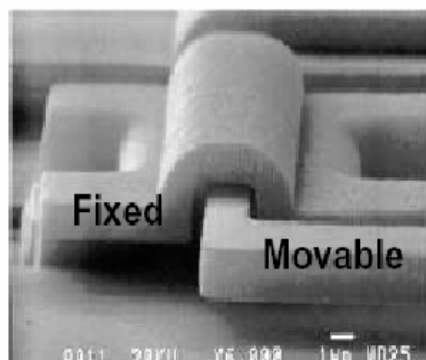


Fig. 3-3 微絞鏈 SEM 圖

為了固定組裝後的微光柵於 90 度的位置上，因此設計一組止動微結構。當底層微光柵被翻起時，位於上層的 I 型懸臂樑因型變產生下壓的力量，並往預先設計好的凹槽進入，當到達設定角度時，I 型懸臂樑滑入凹槽而卡住翻起的微光柵外框完成組裝動作，I 型懸臂樑的長度與凹槽高度及微光柵間距成三角函數關係。Fig. 3-4 為止動結構光罩設計圖，Fig. 3-5 為止動結構三角函數關係。

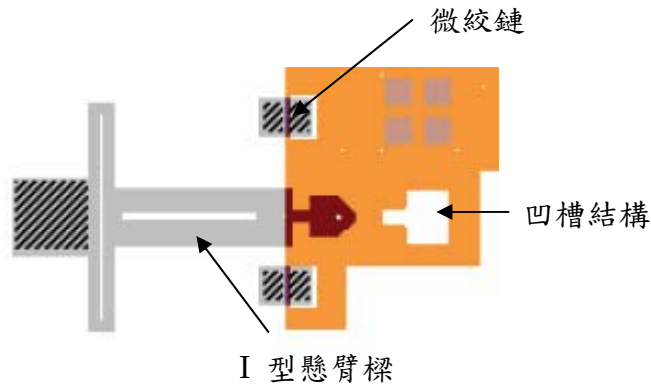


Fig. 3-4 止動微結構光罩設計圖

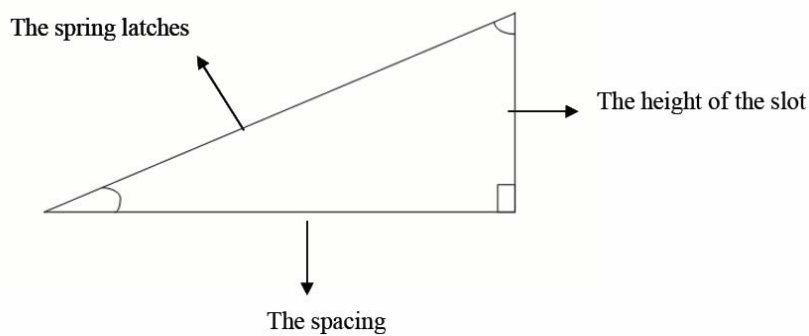


Fig. 3-5 I 型懸臂樑的長度與凹槽高度及微光柵間距的三角函數關係

3-2 微極化分光器之建立與分析

3-2-1 極化分光之計算

極化分光器設計比光柵計算簡單很多，光束從自由空間（空氣介質）入射介電材料產生透射與反射，依循光學斯乃爾定律會產生透射與反射，當入射角為布魯斯特角時入射光 p 分量會完全穿透。在此我們使用 LPCVD 成長之 Low stress 的單層 SiN 薄膜為分光器主體，對於紅光（波長 633nm）折射率 $n=2.13$ ，而吸收率 $k=0.0065$ ，由此可見此種材料對於紅光吸收很小，可維持極高的透光率。計算薄膜厚度參數前，首先我們須先確定此材料與空氣的確切布魯斯特角值，且角度誤差必須考慮進去，我們計算紅光(波長 633nm)從空氣入射折射率 $n=2.13$ ，吸收率為 $k=0.0065$ 的 Low stress 單層 SiN 薄膜的情況下，入射角度與 p 分量（TM 分量）的穿透率關係。入射角為布魯斯特角 64.85° 時穿透率為 100%；有吸收情況下($k=0.0065$)的穿透率亦在布魯斯特角處達到最大 94%，且在該入射角度 $\pm 10^\circ$ 範圍內仍有高達 80% 以上的穿透率，與製程組裝上 $\pm 2^\circ$ 的誤差比較是可以接受的範圍。在布魯斯特角入射條件下，理想 p 分量應當完全穿透薄膜。針對極化分光器，我們希望 s 分量能完全反射至另一方向達到極化分光的功能，對此薄膜厚度為很重要之參數。我們計算紅光 s 分

量在布魯斯特角度入射下改變薄膜厚度與反射率之關係，可發現反射率為薄膜厚度的週期性函數，配合製程鍍膜範圍，我們計算 380nm~430nm 厚度之 low stress SiN 對紅光 p 分量穿透率與 s 分量反射率，Fig. 3-6 及 Fig. 3-7 為計算結果。

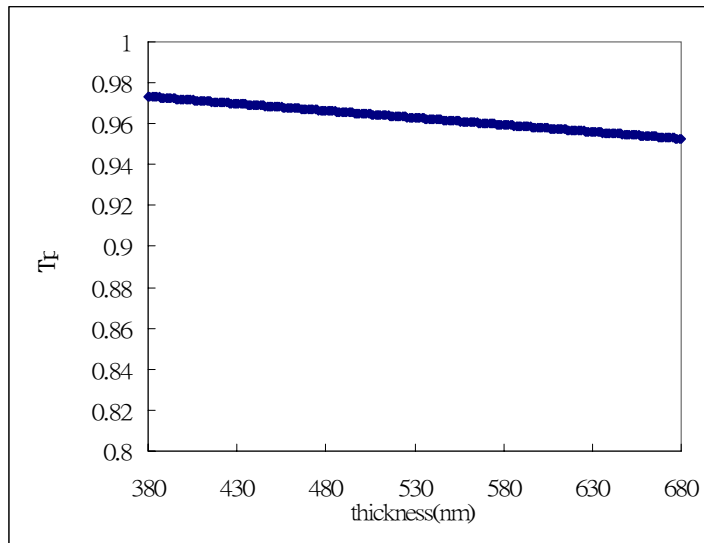


Fig. 3-6 P 分量(TM mode) 膜厚度對穿透率關係計算結果

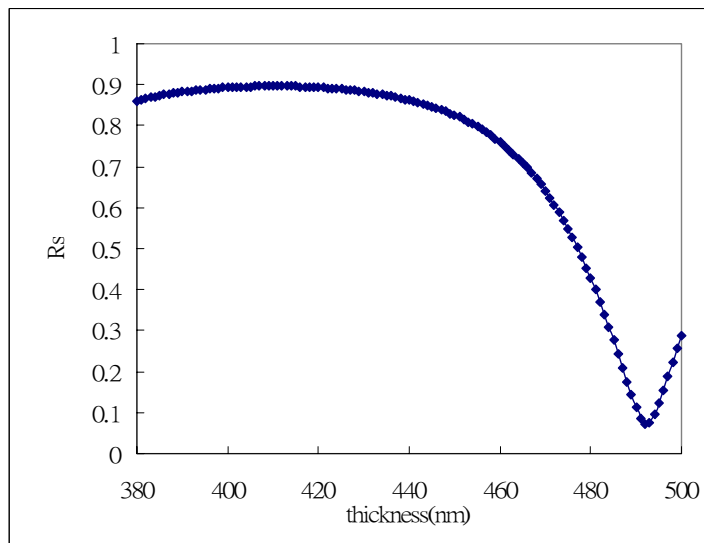


Fig. 3-7 S 分量(TE mode)膜厚度對穿透率關係計算結果

Fig. 3-6 中可發現膜厚度越大 P 分量透射比例越低，是因為吸收率 $k=0.0065$ 的關係，不過穿透率皆可達到 94% 以上。而 S 分量反射率為薄膜厚度週期函數類似弦波上下震盪，Fig. 3-7 只顯示 380nm~430nm 厚度之間關係，故只看得出部分起伏，為得到最大 S 波反射效率，我們選擇 410nm 為預設膜厚，而 390nm~430nm 之間仍有 80% 的效率，此範圍可當作為製程誤差可容忍範圍。

3-2-2 自動組裝定位機構設計

直立式微極化分光器的定位機構設計我們使用和微光柵不同之方法。前者微絞鏈需要人工操作來組裝以及定位，Syms et al.[5]等人利用光阻加溫再流動(reflow)時光阻被液化產生的表面張力將平面之微光學元件拉起，Fig. 3-8 為其設計，我們效法此自動組裝方式在微極化分光器上。

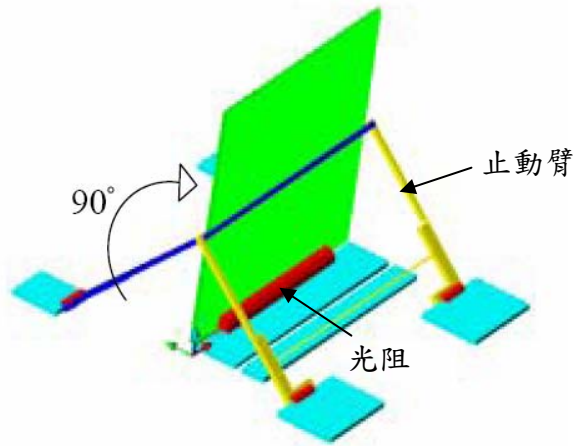


Fig.3-8 Syms 等人利用再流動光阻組裝微鏡面

此方法利用光阻的表面張力為組裝的原動力取代傳統微絞鏈，在光學 SiN 薄膜及 Poly Si 構成的微框架製作完成後將光阻佈於原微絞鏈處，掏空元件下方犧牲層後加熱使光阻液化再流動將懸浮元件拉起，另外由特別設計之止動臂將元件固定至與水平夾角 90 度處，Fig. 3-9 顯示我們的自動組裝機構設計。

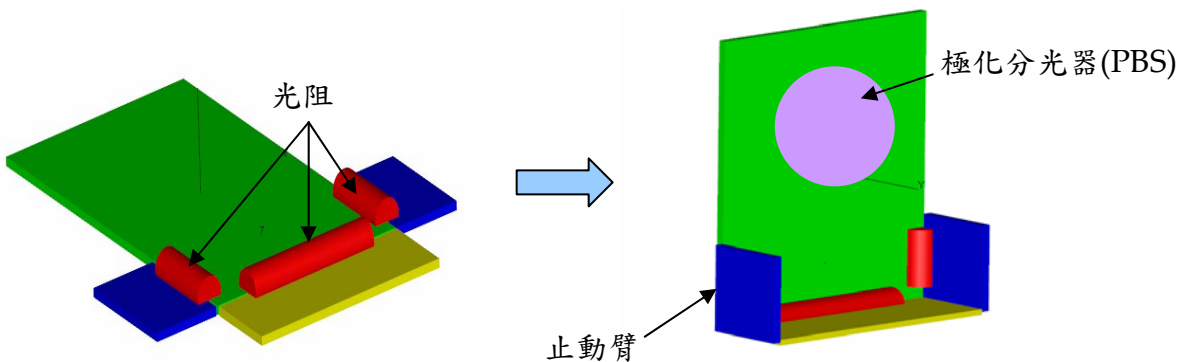


Fig. 3-9 自動組裝之微極化分光器組裝過程示意圖

四、微光柵及微極化分光器的微光學平台製程與結果

4-1 微光柵製造與結果

4-1-1 微光柵製程

實驗中，我們使用 MUMPs-like 技術，其中包括七道光罩微影過程，共五層結構：兩層犧牲層、兩層結構層及一層光學膜，製作流程如下：

- (1) PECVD SiO₂ 沉積：以 PECVD 沉積 SiO₂ 作為第一層犧牲層。MUMPs 稱 PSG-1。
 - (2) Dimple & Anchor-1 光罩：以 Dimple 及 Anchor-1 定義出第一層犧牲層圖形。
 - (3) LPCVD Poly-Si 及 Poly-1 光罩：以 LPCVD 成長 Poly-Si 作為第一層結構層，並以 Poly-1 光罩定義出其圖形。此為微光柵框架結構主體。
 - (4) LPCVD SiN 及 Nitride 光罩：以 LPCVD 成長 SiN 作為光柵材料，並以 Nitride 光罩定義出光柵結構，光柵厚度及線寬在此步驟決定。
 - (5) PECVD SiO₂ 沉積及 Anchor-2：PECVD 第二層 SiO₂ 為第二層犧牲層，並用 Anchor-2 光罩定義出其圖形。
 - (6) LPCVD Poly-Si 及 Poly-2 光罩：以 LPCVD 成長 Poly-Si 作為第二層結構層，並以 Poly-2 光罩定義出其圖形。此為微絞鏈及定位懸臂結構。
 - (7) Release 及定位：使用 HF 將兩層犧牲層洗去，用探針將元件挑起定位於 90 度。
- 製作流程可參考 Fig. 4-1。

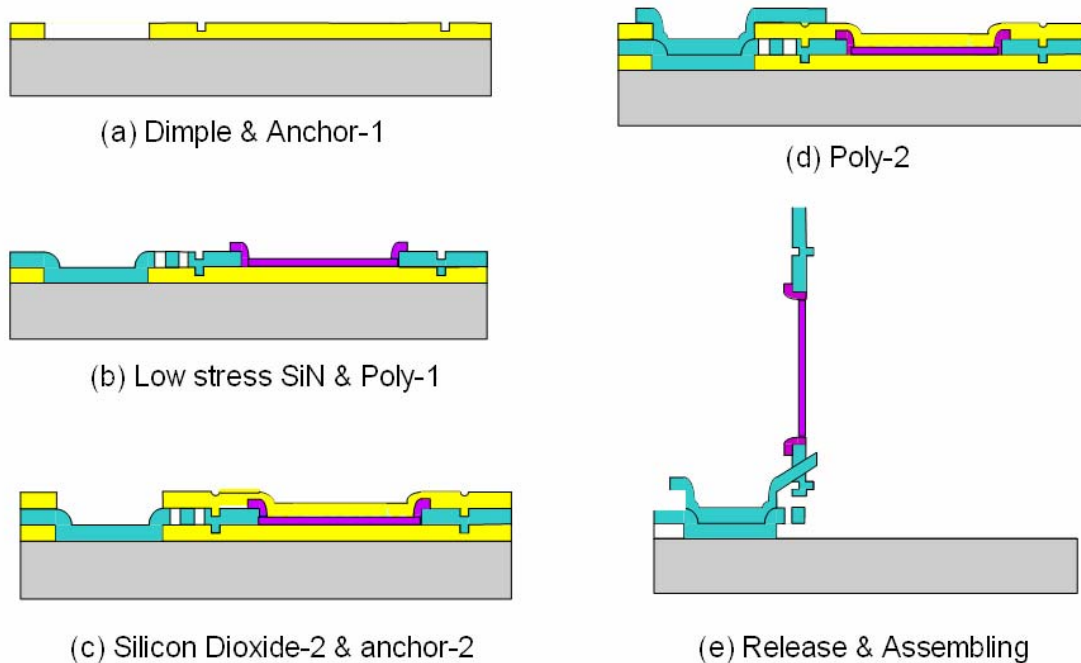


Fig. 4-1 微光柵製作流程示意圖

4-1-2 實驗結果與量測

利用上一節所述之製程，我們成功在矽基板上做出直立式微光柵，Fig. 4-2 為元件 SEM 圖。不過此種微紋鏈式直立式元件製程後定位結構材料應力造成彎曲的問題及製程誤差，其元件角度並不是很準確固定在 90 度，會有 ± 5 度的傾斜。

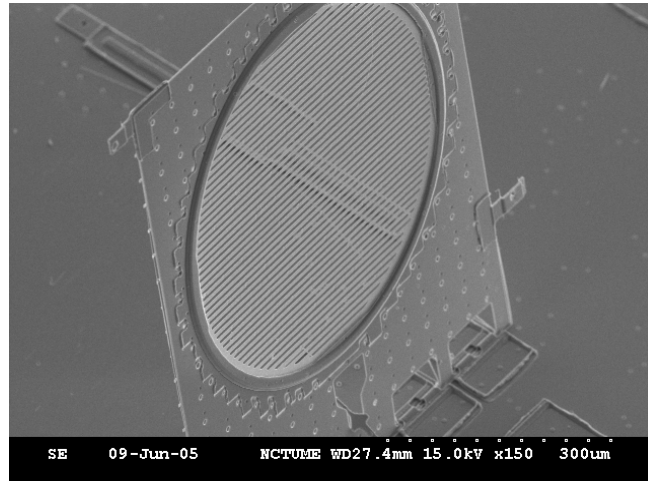


Fig. 4-2 直立式微光柵 SEM 圖

使用氦氖紅光雷射做光柵分光比量測，Fig. 4-3 為量測系統架構圖，Table 4-1 為取三成品的量測結果。由於製程厚度誤差、光柵線寬誤差、元件角度誤差，繞射分光比與計算值有些許不同，不過結果皆在預期範圍內。

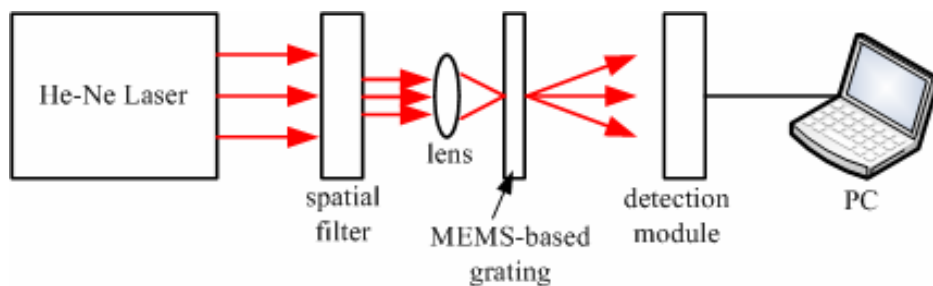


Fig.4-3 量測系統架構圖

Table 4-1 量測結果

Sample No.	Depth (nm)	Fill Factor	-1st order (mw)	0th order (mw)	1st order (mw)	Measured Diffraction efficiency Ratio	Calculated Diffraction Efficiency Ratio
1	~445	~0.43	0.44	1.78	0.42	4.15	3.46
2	~455	~0.56	0.32	1.71	0.32	5.30	4.46
3	~460	~0.45	0.45	1.76	0.43	4.08	4.67

4-2-1 微極化分光器製程

實驗中，我們利用光阻加溫再流動(reflow)時光阻被液化產生的表面張力之自動組裝技術，其中包括四道光罩微影流程，共三層結構：一層犧牲層、一層結構層及一層光學膜，製作流程如下：

- (8) PECVD SiO₂ 沉積：以 PECVD 沉積 SiO₂ 作為犧牲層。
- (9) Dimple 光罩：以 Dimple 定義犧牲層上 Dimple 微孔。
- (10) LPCVD Poly-Si 及 Poly 光罩：以 LPCVD 成長 Poly-Si 作為結構層，並以 Poly 光罩定義出其圖形。此為微光柵框架結構主體。
- (11) LPCVD SiN 及 Nitride 光罩：以 LPCVD 成長 SiN 作為分光器材料，並以 Nitride 光罩定義出薄膜結構。薄膜厚度沉積時就要控制。
- (12) 絞鏈光阻塗佈及絞鏈光罩：塗佈 reflow hinge 光阻，且使用絞鏈光罩定義在絞鏈位置。

製作流程如 Fig. 4-4。

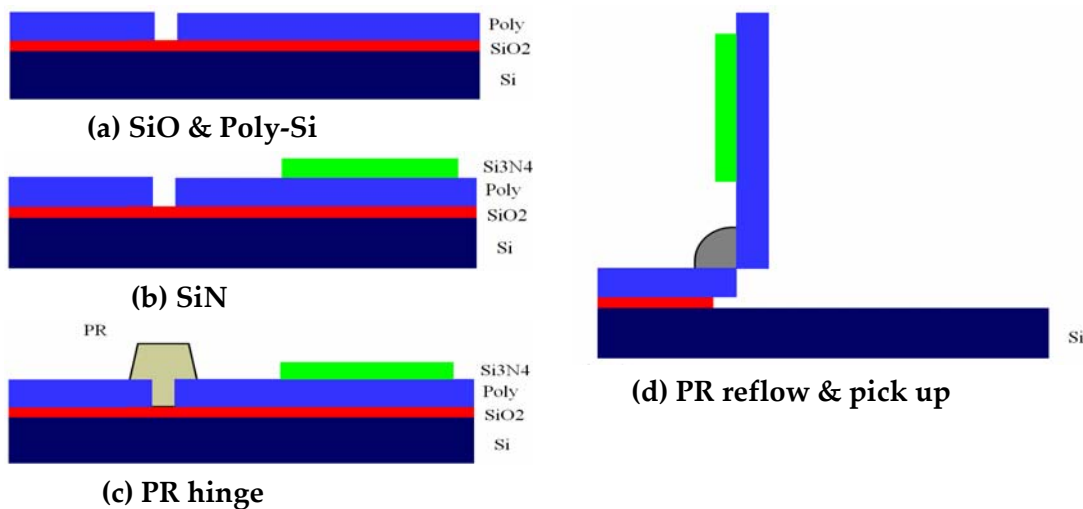


Fig. 4-4 微極化分光器製作流程示意圖

4-2-2 實驗結果與量測

利用上一節所述之製程，我們成功在矽基板上做出直立式微極化分光器，Fig. 4-5 為微極化分光器 SEM 圖。

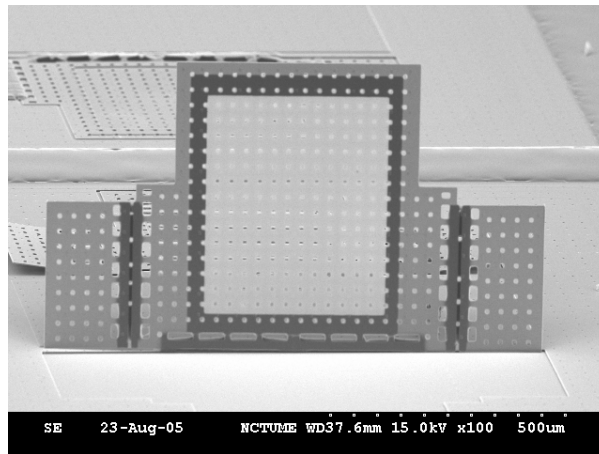


Fig. 4-5 微極化分光器

使用氦氖紅光雷射做分光比量測，Fig. 4-6 為量測系統架構圖，Table 4-2 列出 417nm 膜厚(理想 410nm)下的分光效率，我們做出之元件達到極高的分光比例。

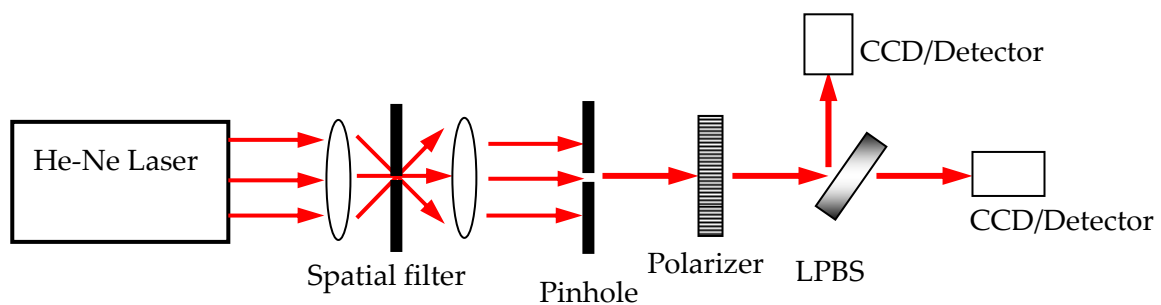


Fig. 4-6 PBS 量測系統架構圖

Table 4-2 417nm 厚度之 SiN 分光效率

Reflectance (TE)	Transmittance (TM)	Reflected Light Extinction Ratio (dB)	Transmitted Light Extinction Ratio (dB)
83.3 %	99.7 %	20.9	9.6

4-2-3 etch hole 效應

此次在量測微極化分光器效率時，光束以類高斯場型入射極化分光器，當光束穿過或反射於極化分光器薄膜後光場不再是類高斯場型，量測到的是類似光穿過週期性排列之圓孔產生的繞射圖案，這不是預期的結果，有人對此結果做出討論[7]~[9]。探究原因是由於直立微光學元件在釋放犧牲層時為確保片狀元件完全懸浮，製程上需要在片狀元件上佈局約 3~5 μm 大小之微孔以利 HF 確實透過結構至元件下方進行二氧化矽的蝕刻，此種孔洞微機電製程上我們稱做蝕刻孔(etch hole)。

蝕刻孔的佈局為了光罩製圖方便一般我們以週期性規則排列。但在直立式光學平台上，由遠場繞射理論解釋[10]，凡光束經過週期性排列結構會在成像平面上呈現出多階光束的繞射圖形，而每一階光束在像平面會有愛里斑(Airy Disc)分布，故在一般週期性分佈蝕刻孔的微光學元件在光束經過後會造成二維多階繞射圖形[11]，Fig. 4-7 為此微極化分光器透射光光場圖形。

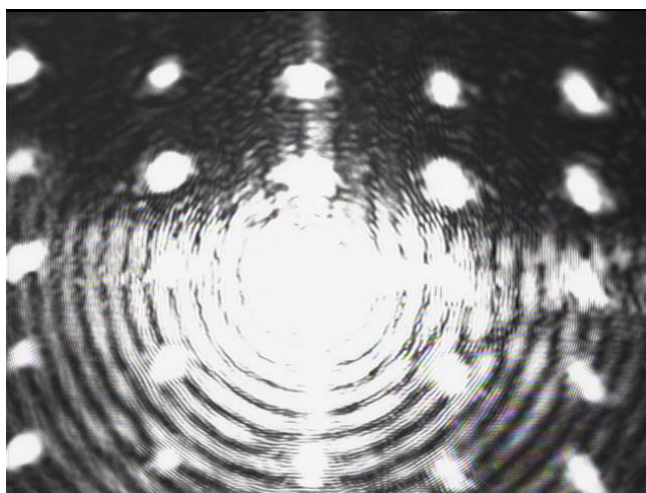
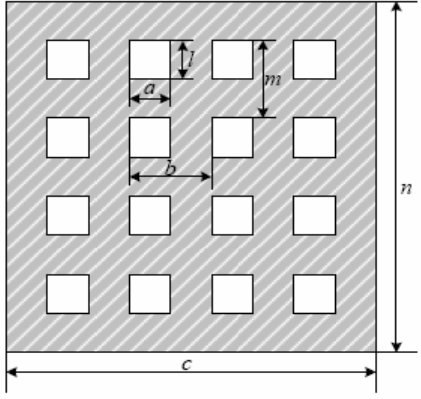

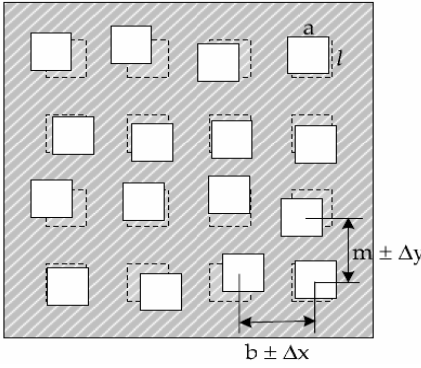
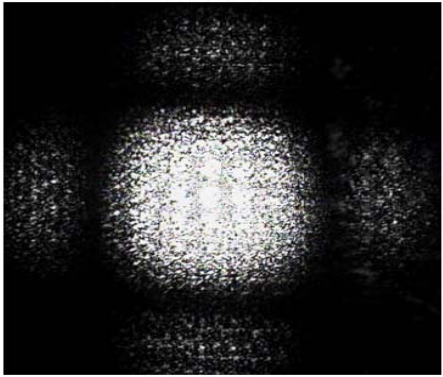
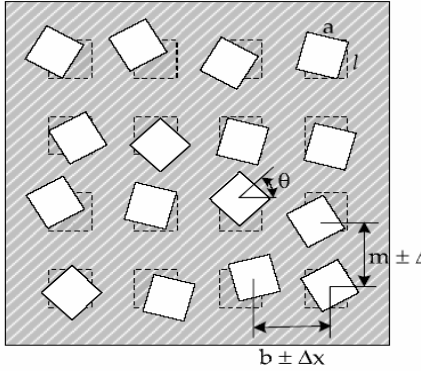
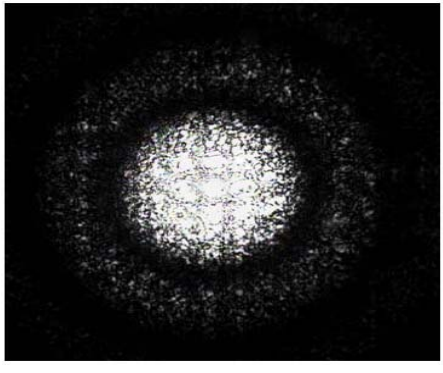


Fig. 4-7 微極化分光器透射光光場分佈

直立式微光學元件蝕刻孔產生的多階繞射圖形在實際應用上是沒有必要的，尤其光束經過多道元件的微光學平台，多餘的繞射分光會使最終出光效率低弱。對於此針對單一元件減少蝕刻孔的繞射是必要的，我們對於不同分佈蝕刻孔的直立式微鏡片做繞射圖形的討論，Table 4-3顯示我們針對週期性、隨機平移及任一旋轉排列蝕刻孔量測之光場型歸納，此討論結果及詳細繞射數學式我們已投稿至期刊 *Journal of IEEE. Microelectromech. Syst.* 請參考附錄。

Table 4-3 不同排列方式蝕刻孔對應量測結果

蝕刻孔排列方式	量測結果	
<p>規則 週期</p> 		
<p>隨機 平移</p> 		
<p>平移 旋轉</p> 		

五、未來研究方向及目標

在未來研究中，我們將繼續利用此種微機電光學平台技術，進而製作及討論其應用可行性：

(1) 簡化製程步驟：

我們將充分利用自動組裝技術製造各種光學元件，並從中發展出更簡化之自動組裝技術，符合工業製造需求。

(2) 加入微旋轉平台及微至動器：

目前微型直立元件製作已成熟，進而將整合微型旋轉基座及微動器，發展出更可廣泛應用之元件。

(3) 改善蝕刻孔佈局：

我們將繼續研究刻孔佈局對於光學繞射影響，並改善其佈局達到較好的出光效率，使其更符合應用需求。

(4) 製作高階繞射元件：

進而利用電子束微影技術製作次波長光柵及各種高階之繞射元件，發展更多光學上的應用。

六、結論

本次計畫中，我們在微機電平台上製作了具有一階分光功能之直立式微光柵及極化分光功能之微分光器，量測結果與計算結果誤差均在可預測範圍內。微機電製程複雜，誤差來源皆來自製造上的差異性。

我們更成功嘗試自動組裝技術減少製造上差異，並探討光學在微機電結構上的效應。目前此技術皆還在前瞻研究階段，未來我們將朝實際應用方向努力。

七、計畫成果自評

本研究大致完成計畫書中所提出之研究項目，除了受限於經費與機台線寬，所製作的微光柵及微極化分光器線寬最小值為 $3\ \mu\text{m}$ 。我們並已將不同分佈蝕刻孔的直立式微鏡片繞射圖形的研究結果投稿於 *Journal of Microelectromechanical Systems* 與 *Japanese Journal of Applied Physics* 兩篇期刊。

八、參考文獻

- [1] K.S.J., etc., "Microfabricated hinges," *Sensors and Actuators*, A33, pp. 249-256 (1992).
- [2] M.C.Wu, etc., "Micro-machined Free-space Integrated Micro-optics," *Sensors and Actuators*, vol.50, pp. 127-134 (1995).
- [3] D. Koester, A. Cowen, R. Mahadevan, and B. Hardy, *PolyMUMPs Design Handbook* Revision 10.0.
- [4] 國立中央大學光電所 黃裕龍碩士論文
- [5] R.R.A. Syms, etc. "Improving yield, accuracy and complexity in surface tension self-assembled MOEMS," *Sensors and Actuators*, A, 88, pp. 273-283 (2001).
- [6] E. Smela, L. Inganas, and I. Lundstrom, "Controlled folding of micrometer-size structures," *Science*, Vol. 268, pp. 1735-1738 (1995).
- [7] W. N. Sharpe, Jr., R. Vaidyanathan, B. Yuan, G. Bao and R. L. Edwards, "Effect of etch holes on the mechanical properties of polysilicon," *J. Vac. Sci. Technol.* Vol. B 15, pp. 1599-1603 (1997).
- [8] X. Fang, N. Myung, K. Nobe, and J. W. Judy, "Modeling the effect of etch holes on Ferromagnetic MEMS," *IEEE Tran. on Magnet.* Vol. 37, pp. 2637-2639 (2001).
- [9] J. Zou, M. Balberg, C. Byrne, C. Liu, and D. J. Brady, "Optical properties of surface micromachined mirrors with etch holes," *IEEE J. Microelectromech. Syst.*, Vol. 8, pp. 506-513 (1999).
- [10] J. W. Goodman, *Introduction to Fourier Optics* (McGraw-Hill, Singapore), pp. 35-36.
- [11] K. Iizuka, *Elements of Photonics* (Wiley-Interscience, New York, USA), pp. 32-40

附錄

學術論文

[1] Chung-Hao Tien, Yen-Hsing Lu and Chien-Hsiang Hung, "Effect of etch holes on the properties of surface micromachining," submitted to *Journal of Microelectromechanical Systems*.

[2] Chung-Hao Tien, Chi-Hung Lee, "Optical properties of surface micromachining with randomly distributed etch holes," submitted to *Japanese Journal of Applied Physics*.

Effect of etch holes on the optical properties of surface micromachining

Chung-Hao Tien, Yen-Hsing Lu, and Chien-Hsiang Hung

Department of Photonics and Display Institute, National Chiao Tung University,

Hsinchu, Taiwan, 30010

Tel: 886-3-5131584, Fax: 886-3-5737681, E-mail: chtien@mail.nctu.edu.tw

When wet etches are used to release the microstructure, it is common to distribute small etch holes over the surface to minimize the duration so that all undesirable etching of other films or structures shall be reduced. However, the arrangement and form factor of the etch-holes array strongly affect the optical properties of such perforated structures. In this paper, a model based on Fraunhofer diffraction theory is presented to study the dependence of diffraction behavior on various etch-holes array. Comparison with experimental results confirms the validity of this model.

Index Terms – Etch holes, surface micromachining, Fraunhofer diffraction theory.

1. Introduction

Microoptics have expanded widely over the last decade in terms of their diverse applications in device and instrumentation. For most applications, integration of discrete optical components into a fully function system is crucial, in order to reduce size and cost, as well as to enhance the robustness and stability. The micromachining, or microelectromechanical systems (MEMS) technology can implement a functional system to be monolithically integrated on a single chip via a VLSI-like process (VLSI: very large scaled integrated), thus provides a potential route to meet such requirements. In addition, mechanical components such as hinged and rotating structures combined with a compact microactuator allow a moveable function in operating. This advantage can performe more complex function and has been widely applied in many optical systems such as optical display, data storage, switches, and sensors.¹⁻⁴

Among various MEMS fabrication technologies, surface micromachining process, on which alternating layers of structural and sacrificial materials can be deposited and patterned to create various structures, are the most popular approach for its integrated circuit (IC)-like foundry process.⁵⁻⁶ For surface micromachining process, the most well known recipe is to use polysilicon as the structural material and silicon oxide as the

sacrificial material due to the excellent mechanical properties of polysilicon and high selectivity of sacrificial etching with hydrofluoric acid. As the sacrificial etching process is facilitated to release a large-area microstructure, it is common to distribute an etch-holes array over the microstructure to minimize the duration so that all undesirable etching of other films or structures shall be reduced. One example of a free-space optical reflector is shown in Fig. 1, where etch holes are periodically spaced in a two-dimensional array. These etch holes are inevitable for free-space features under surface micromachining technologies. The effects of the etch-holes array on the electromechanical and ferromagnetic properties have been discussed before.⁷⁻⁸ However, only a few papers have been dedicated to the behavior of diffraction, and they mainly reported this topic numerically and lack an analytical consideration.⁹ In this paper, we first describe the diffraction from a perforated thin film with a square etch-holes array, which is the most typical mask layout in the surface micromachining process (Section 2). In Section 3, we propose applying a random distributed etch holes layout to eliminate the high-order diffracted beam without loss of fabrication convenience. In Section 4, the experiment is setup and compared with the calculated values. Finally, a conclusion and discussion is given (Section 5).

2. Diffraction from Etch-holes Array with Regular Spacing

The diffraction caused by a two-dimensional (2D) etch-holes array is analogous to the case in which a uniform plane wave is diffracted by a crossed grating. In this case, the features on the perforated film are treated as scalar phase/amplitude objects. This means that the incident beam is simply modulated by a complex transmission (or reflection) coefficient introduced by the properties of microstructure with etch-holes array. Here we ignore the physics of interaction between the etch hole and the incident beam in the conformity with the relief pattern and assume aperture part merely imports to the incident beam an amplitude modulation. Despite the fact that solving the Maxwell equation is most exact way for diffraction analysis, approximating etch holes as amplitude objects holds well for our case where typical aperture sizes of MEMS structure are much larger than the working wavelength. In addition, we can avoid entailed massive computations and get a fast calculation. The wavelength λ for the simulation is 633 nm. However, as long as two conditions are met (1) the diffracting etch hole must large compared with wavelength, and (2) the diffracting fields must not be observed too close to the aperture,¹⁰ the calculated values can be applied to different wavelengths by scaling all the geometry parameters involved proportionally. Fig. 2 illustrates the transmission function $B(x,y)$ of a perforated die and geometric parameters for diffraction calculation. If the overall size of the die is limited to $c \times n$, etch holes have a size of $a \times l$ and are spaced b and m apart in the x and y directions, respectively, then the transmission function of the etch-holes array can be expressed as

$$B(x, y) = \left[\Pi\left(\frac{x}{a}\right) * \text{III}\left(\frac{x}{b}\right) \right] \Pi\left(\frac{x}{c}\right) \times \left[\Pi\left(\frac{y}{l}\right) * \text{III}\left(\frac{y}{m}\right) \right] \Pi\left(\frac{y}{n}\right) \quad (1)$$

where $\Pi(x/a)$ is a rectangular function of width a . The function for such an aperture is defined as

$$\Pi\left(\frac{x}{a}\right) = \begin{cases} 1 & |x| \leq \frac{a}{2} \\ 0 & |x| > \frac{a}{2} \end{cases} \quad (2)$$

and $\text{III}(x/b)$ is a comb function of spacing b . The transmission function of comb function can be written as

$$\text{III}(x, b) = \sum_{k=-\infty}^{\infty} \delta\left(\frac{x}{b} - k\right) = b \sum_{k=-\infty}^{\infty} \delta(x - kb) \quad (3)$$

Note that etch-holes array with regular spacing can be generated by convolving the rectangular function $\Pi(x)$ with $\text{comb}(x)$. In this paper, the convolution operator is denoted by a symbol “*”. For a typical MEMS device where propagation distance z is much larger compared with x' , y' , the diffraction by 2D etch-holes array can be estimated using Fraunhofer diffraction formula, by which the diffracted pattern is obtained as the Fourier transform of the transmission function, that is $F\{B(x)\} = E(f_x, f_y)$,

where the argument $f_x = \sin\theta_x/\lambda \approx x'/\lambda z$ and $f_y = \sin\theta_y/\lambda \approx y'/\lambda z$, as shown in **Fig. 2**. The

Fourier transform of the comb function is

$$F\{\text{III}(x, b)\} = b \sum_{k=-\infty}^{\infty} \text{III}(f_x, \frac{1}{b}) \quad (4)$$

Consequently, we can obtain the amplitude distribution of the wave diffracted through the perforated film

$$\begin{aligned} E(f_x, f_y) &= F\{B(x, y)\} \\ &= F\left\{\Pi\left(\frac{x}{a}\right)\right\} \left[F\left\{\Pi\left(\frac{x}{c}\right)\right\} * F\left\{\text{III}(x, b)/b\right\} \right] \times F\left\{\Pi\left(\frac{y}{l}\right)\right\} \left[F\left\{\Pi\left(\frac{y}{n}\right)\right\} * F\left\{\text{III}(y, m)/m\right\} \right] \\ &= \text{asinc}(af_x) [\text{csinc}(cf_x) * \text{III}(f_x, 1/b)] \times \text{lsinc}(lf_y) [\text{nsinc}(nf_y) * \text{III}(f_y, 1/m)] \\ &= \text{asinc}(af_x) \left[\frac{c}{b} \text{sinc}(cf_x) * \sum_{k_x=-\infty}^{\infty} \delta\left(f_x - \frac{k_x}{b}\right) \right] \times \text{lsinc}(lf_y) \left[\frac{n}{m} \text{sinc}(nf_y) * \sum_{k_y=-\infty}^{\infty} \delta\left(f_y - \frac{k_y}{m}\right) \right] \\ &= \text{alsinc}(af_x) \text{sinc}(lf_y) \left[\sum_{k_x=-\infty}^{\infty} \sum_{k_y=-\infty}^{\infty} N_x N_y \text{sinc}\left(c\left(f_x - \frac{k_x}{b}\right)\right) \times \text{sinc}\left(n\left(f_y - \frac{k_y}{m}\right)\right) \right] \end{aligned} \quad (5)$$

where N_x and N_y are the number of etch holes in the x and y directions, respectively.

Figure 3 shows the irradiance distribution of a square etch-holes array with $a = l = 5 \mu\text{m}$, $b = m = 20 \mu\text{m}$ and $c = n = 200 \mu\text{m}$. Because the order of the dimension in the transmission pattern is $a < b < c$, the order of the diffracted pattern which is the Fourier transform of the etch-holes array has an inverse relationship; namely,

$$\frac{1}{c} < \frac{1}{b} < \frac{1}{a} \quad (6)$$

where $1/c$ is the size of an individual spot, $1/b$ is the spacing between each spikes, and $1/a$ is the overall size of the diffraction pattern.¹¹ When the ratio of the aperture width a and the period b is an integer, the minimum of the envelope will exactly coincide with some of the spikes of the array pattern. In this case, $b/a = 4$, the fourth spikes overlaps with the first null of side lobe and the intensity of the fourth spike thus disappears. Since the intensity distribution is obtained as

$$I(f_x, f_y) = E^*(f_x, f_y)E(f_x, f_y) \quad (7)$$

accordingly, we can calculate the intensity

$$\begin{aligned} I &= I_0 \text{sinc}^2(af_x) \text{sinc}^2(lf_y) \left[\sum_{k_x=-\infty}^{\infty} \sum_{k_y=-\infty}^{\infty} \text{sinc}^2\left(c\left(f_x - \frac{k_x}{b}\right)\right) \text{sinc}^2\left(n\left(f_y - \frac{k_y}{m}\right)\right) \right] \\ &= I_0 \text{sinc}^2(af_x) \text{sinc}^2(lf_y) \left[\frac{\sin(\pi cf_x)}{N_x \sin(\pi bf_x)} \right]^2 \left[\frac{\sin(\pi nf_y)}{N_y \sin(\pi mf_y)} \right]^2 \end{aligned} \quad (8)$$

where

$$\begin{aligned} \sum_{k_x=-\infty}^{\infty} \text{sinc} \left[c \left(f_x - \frac{k_x}{b} \right) \right] &= \frac{\sin(\pi cf_x)}{N_x \sin(\pi bf_x)} \\ \sum_{k_y=-\infty}^{\infty} \text{sinc} \left[n \left(f_y - \frac{k_y}{m} \right) \right] &= \frac{\sin(\pi nf_y)}{N_y \sin(\pi mf_y)} \end{aligned} \quad (9)$$

which can be verified through the serial expansion

$$\frac{1}{\sin x} = \sum_{k=-\infty}^{\infty} \frac{(-1)^k}{x - \pi k} \quad (10)$$

Consequently, the intensity can be represented in this form

$$I = I_0 \frac{\sin^2 \alpha_x}{\alpha_x^2} \frac{\sin^2 \alpha_y}{\alpha_y^2} \left[\frac{\sin(N_x \beta_x)}{N_x \sin \beta_x} \right]^2 \left[\frac{\sin(N_y \beta_y)}{N_y \sin \beta_y} \right]^2 \quad (11)$$

where

$$\alpha_x = \frac{\pi}{\lambda} a \sin \theta_x, \alpha_y = \frac{\pi}{\lambda} l \sin \theta_y$$

$$\beta_x = \frac{\pi}{\lambda} b \sin \theta_x, \beta_y = \frac{\pi}{\lambda} m \sin \theta_y \quad (12)$$

It can be seen from Eq. (11) that the diffracted pattern is contributed by two factors of different natures. The factors outside the square brackets are determined solely by the shape of aperture element and are called the shape factor, which appears as the envelope of the diffraction pattern. On the other hand, the factors inside the square brackets are determined solely by the period and die size of etch-holes array, are called the array factor. The diffracted pattern is the product of these two factors.

Sometimes the actual shape of etch holes after plasma etching tends to be circular rather than square due to imperfect photolithography and etching process. In this case, *sinc* function caused by the rectangular element in Eq. (5) can be substituted by the *Bessel* function, which is the Fourier transform of the circular aperture. Similarly, when the surface area of a microstructure is relatively larger than the illuminated spot size, the overall size is determined by the spot size rather than the external border of the device. Therefore, *sinc* function caused by the rectangular die should be replaced by the *Bessel* function as well.

3. Diffraction from Etch-holes Array with Random Distribution

According to the preceding study, we note that periodicity of the etch-holes array leads to considerable amount of high-order beams. In the above case, the normalized intensity of the lowest few orders are 1 [0th order], 0.8113[(1,0), (0,1) order], 0.6582 [(1,1) order], 0.4072 [(2,0), (0,2) order]. Such high-order diffraction beams are often undesirable to the optical performance by generating noise and erroneous crosstalk signals in most optical systems. Let us examine an etch-holes layout, where etch holes are randomly arranged but without any rotation of the individual elements, as shown in Fig. 4 (a), where the dash lines represent the original position of each etch hole and solid lines represent the random offset from the original one. For simplicity, we ignore the external border and

only consider one-dimensional case. If each square aperture is translated in the x direction by a random distance b_k from its original position, then the transmission function can be represented by

$$B(x) = \sum_{k=0}^{N_x-1} \Pi\left(\frac{x-b_k}{a}\right) \quad (13)$$

where the translated distance b_k are generated by the computer according to discrete uniform distribution.¹² Using the shift property of the Fourier transform,

$$F\{h(x \pm b_k)\} = e^{\mp j2\pi f_x b_k} H(f_x) \quad (14)$$

The amplitude distribution in far field can be expressed by

$$E(f_x) = \text{sinc}(af_x) \left[1 + e^{-j2\pi b_1 f_x} + e^{-j2\pi b_2 f_x} + e^{-j2\pi b_3 f_x} + \dots \right] \quad (15)$$

Therefore

$$I = E^* E = \text{sinc}^2(af_x) \left(N_x + 2 \sum_{j=1}^{N_x-1} \sum_{k=1}^{N_x-1} \cos 2f_x (b_j - b_k) \right) \quad (16)$$

Since b_j and b_k are random in this case, the translation corresponds to a superposition of cosine functions with a random period, which leads the interference term in Eq. (16) to

zero. Such analysis can be extended to 2D case and the intensity of the diffracted wave thus becomes $N_x N_y \text{sinc}^2(af_x) \text{sinc}^2(lf_y)$, as shown in Fig. 4 (b), where the grid pattern due to the array factor is average out and the diffraction pattern is solely determined by the form factor of each element but with N times the intensity.

Although random spacing is an effective approach to eliminate the high-order diffracted beams and thus alleviate the crosstalk effect, one more requirement should be noted when failure mechanisms are taken into consideration.¹³ Because typical surface micromachining uses polysilicon thin film as the structure layer and the silicon oxide thin film as the sacrificial layer. If the spacing of etch holes on the polysilicon layer is too far, the etchant is hard to access the center of the large-area micromechanical structure, thereby failing to release the component. On the contrary, while the spacing is too close, the stress concentration is accumulated around the etch holes and the polysilicon film is easily cracked during the fabrication or assembly process. Therefore, one more condition is needed that the spacing between each etch hole b_k should be limited in the range of $20 \pm 5 \mu\text{m}$ in this case.

We can further randomize each aperture element with respect to rotation angle θ as well as translation, as shown in Fig. 5 (a). Since the form factor of etch holes has been randomized with center symmetry, the calculated irradiance in Fig. 5 (b) looks like one

obtained by rotating the diffracted field of a single square aperture about its center.

4. Experimental Results

To verify the relationship between diffraction and etch-holes layout, we develop a 2D micromirror through MUMPS (Multi-User MEMS Processes).¹⁴ The micromirror contains various etch-holes layouts compatible with MUMPS design rules. The 2- μm polysilicon surface of interest is the *poly 1* layer, produced by low pressure chemical vapor deposition (LPCVD) process on the top of a layer of 2- μm silicon oxide film. Since we aim to study the dependence of diffraction behavior on various etch-holes arrays, the MUMPS mirror is not released from the substrate. The experimental setup is shown schematically in Fig. 6. A He-Ne laser ($\lambda = 633 \text{ nm}$) is directed toward the perforated film after passing through a variable attenuator, a spatial filter, and a collimating lens to emerge as a collimated beam. The beam uniformly fills the entrance pupil of the telescope system and scale the diameter of beam size down to 200 μm . The sample is mounted on a plate riding on a translation stage. An etch-holes array acts as a 2D diffraction grating that diffracts the laser beam into several diffraction orders. The diffraction pattern is captured and analyzed by means of a CCD camera and a personal computer, respectively. The measured irradiance distributions of various etch-holes features are shown in Fig. 7. The measured results make a close agreement with the

previous simulation and qualitatively confirm our theoretical analysis based on Fraunhofer diffraction theory.

5. Conclusions

To summarize, optical MEMS typically require etch holes to reduce the time required to release the micromechanical structure during the sacrificial undercutting. However, the size and density of the etch-holes array has a strong effect on the diffraction patterns, which plays a key role in most optical characteristics. In this paper, we examined the dependence of diffracted pattern on the etch-holes configuration based on an analytical Fourier study. The diffracted irradiance caused by etch-holes array is contributed by two factors, namely, array factor and shape factor. Array factor determined by the period of the etch holes can cause high-order diffraction beams, which can be averaged out by use of random translation layout. On the other hand, the shape factor determined by the form factor of each element provides the envelope of the overall diffraction pattern. The envelop can be centrally symmetrized by the randomly rotation of each element. Optical experiments quantitatively confirmed our analyses. The proposed design of random distributed etch-holes array is expected to provide a useful consideration for future surface micromachining design rule.

Acknowledgement

This work was supported by the National Science Council, the Republic of China under contract no. NSC 94-2215-E-009-028.

References

1. R.L. Knipe, "Challenges of a Digital Micromirror Device: Modeling and Design," *SPIE Europto Proceedings*, Vol. 2783, pp. 135-145, June 1996.
2. M. C. Wu, L. Y. Lin, S. S. Lee, and K. S. J. Pister, "Micromachined free-space integrated micro-optics," *Sens. Actuators: A (Physical)*, Vol. 50, pp. 127-134, 1995.
3. S. S. Lee, L. S. Huang, C. J. Kim, and M. C. Wu, "Free-Space Fiber-Optic Switches Based on MEMS Vertical Torsion Mirrors" *Journal of Lightwave Technol.*, Vol. 17, pp. 7-13, 1999.
4. E. Smela, L. Inganas, and I. Lundstrom, "Controlled folding of micrometer-size structures," *Science*, Vol. 268, pp. 1735-1738, 1995.
5. R. T. Howe and R. S. Muller, "Polycrystalline silicon micromechanical beams," *J. Electrochem. Soc.*, Vol. 130, pp. 1420-1423, 1983.
6. MEMS Technology Applications Center, Microelectronics Center at North Carolina (MCNC), Research Triangle Park, NC, and Integrated Micro Electro Mechanical Systems, offered at Analog Devices, Cambridge, MA.

7. W. N. Sharpe, Jr., R. Vaidyanathan, B. Yuan, G. Bao and R. L. Edwards, "Effect of etch holes on the mechanical properties of polysilicon," *J. Vac. Sci. Technol.* Vol. B 15, pp. 1599-1603, 1997.
8. X. Fang, N. Myung, K. Nobe, and J. W. Judy, "Modeling the effect of etch holes on Ferromagnetic MEMS," *IEEE Tran. on Magnet.* Vol. 37, pp. 2637-2639, 2001.
9. J. Zou, M. Balberg, C. Byrne, C. Liu, and D. J. Brady, "Optical properties of surface micromachined mirrors with etch holes," *IEEE J. Microelectromech. Syst.*, Vol. 8, pp. 506-513, 1999.
10. J. W. Goodman, *Introduction to Fourier Optics* (McGraw-Hill, Singapore), pp. 35-36.
11. K. Iizuka, *Elements of Photonics* (Wiley-Interscience, New York, USA), pp. 32-40.
12. W. H. Beyer, *CRC Standard Mathematical Tables, 28th ed.*, (CRC Press, FL., 1987).
13. J. A. Walraven, "Failure mechanisms in MEMS," *IEEE ITC International Test Conference Paper 33.1*, pp. 828-833, 2003.
14. D. Koester, A. Cowen, R. Mahadevan, and B. Hardy, *PolyMUMPs Design Handbook Revision 10.0*.

Figure captions

Fig. 1. SEM of a microplate with an etch-holes array.

Fig. 2. Illustration of (a) transmission function $B(x,y)$ of a perforated die and (b) geometric parameters for diffraction calculation.

Fig. 3. (a) The distributed pattern of the membrane perforated by a square etch-holes array with $a = l = 5 \mu\text{m}$, $b = m = 20 \mu\text{m}$ and $c = n = 200 \mu\text{m}$ (b) irradiance cross-section, where the order of the pattern has an inverse relationship of the etch-holes layout.

Fig. 4. (a) Geometric parameters of the translated etch holes layout, dash line represents the original position and solid lines represents the random offset by discrete uniform distribution (b) calculated irradiance pattern.

Fig. 5. (a) Geometric parameters of the random distributed etch holes layout, dash line represents the original position and solid lines represents the position after random translation and rotation (b) calculated irradiance pattern.

Fig. 6. Schematic configuration of the measurement system.

Fig. 7. The measured irradiance patterns of various etch-holes features (a) periodic square etch-holes array (b) etch-holes array with random translation (c) etch-holes array with random translation and rotation.

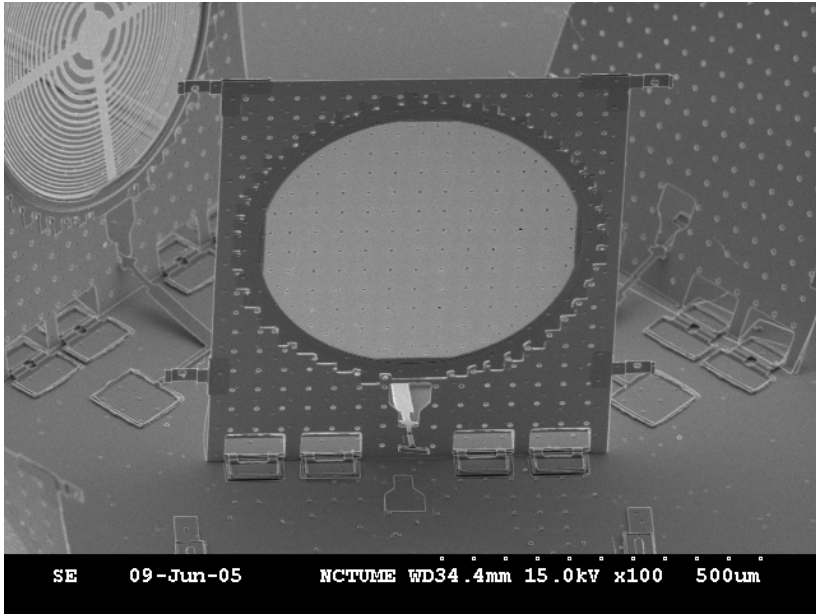


Fig. 1. SEM of a microplate with an etch-holes array.

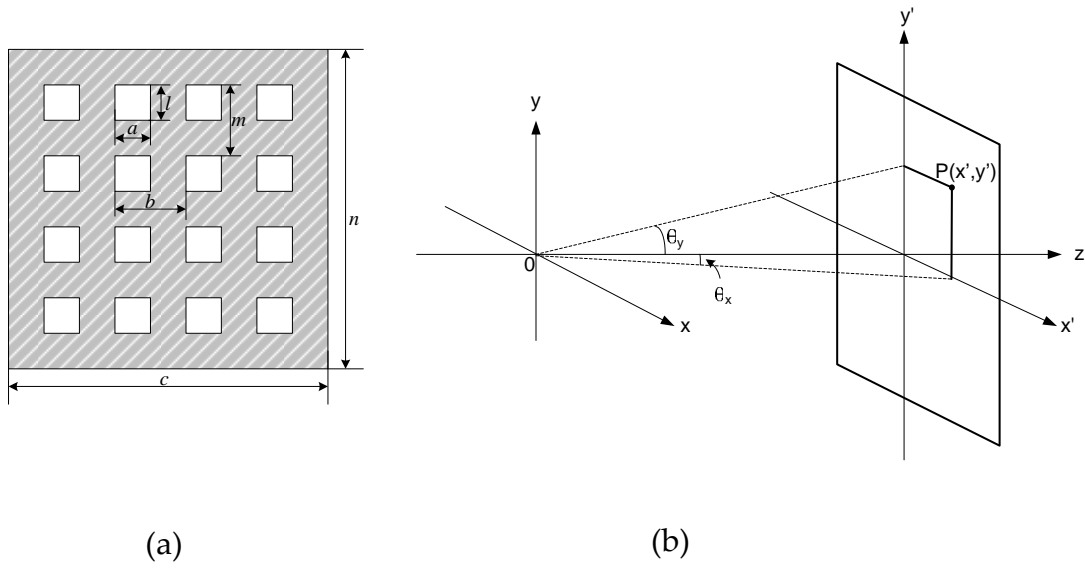
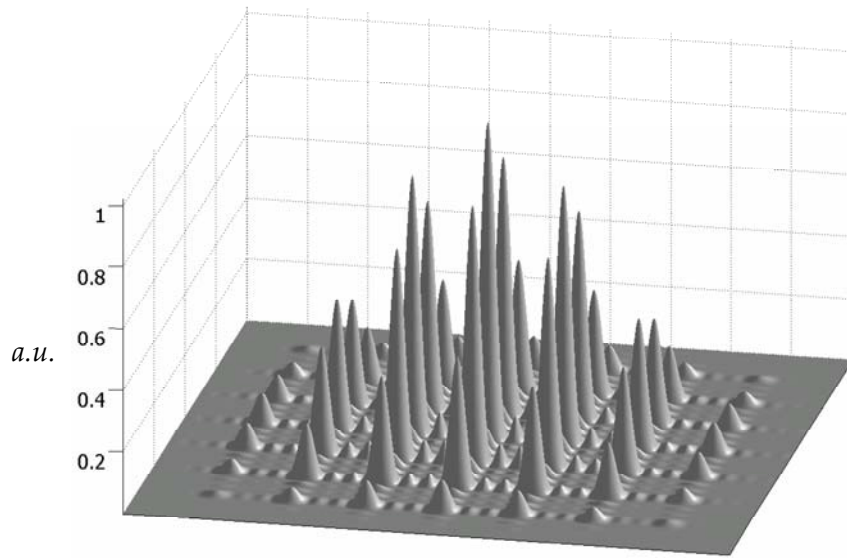
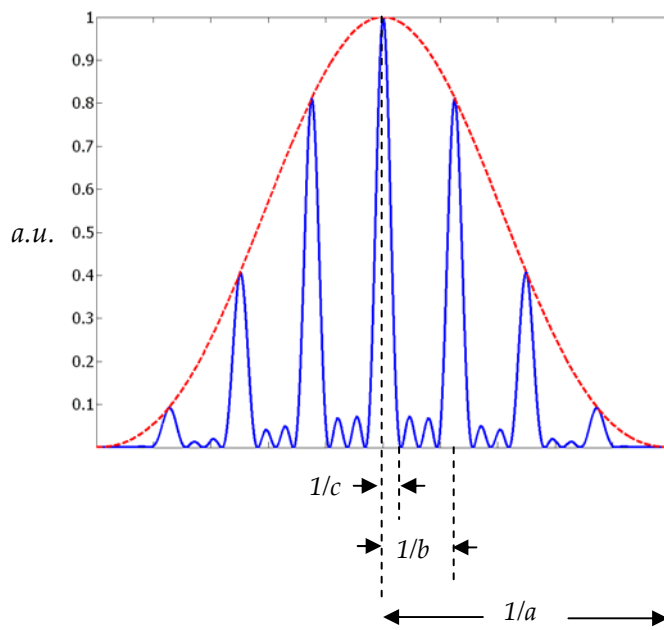


Fig. 2. Illustration of (a) transmission function $B(x,y)$ of a perforated die and (b) geometric parameters for diffraction calculation.



(a)



(b)

Fig. 3. (a) The distributed pattern of the membrane perforated by a square etch-holes array with $a = l = 5 \mu\text{m}$, $b = m = 20 \mu\text{m}$ and $c = n = 200 \mu\text{m}$ (b) irradiance cross-section, where the order of the pattern has an inverse relationship of the etch-holes layout.

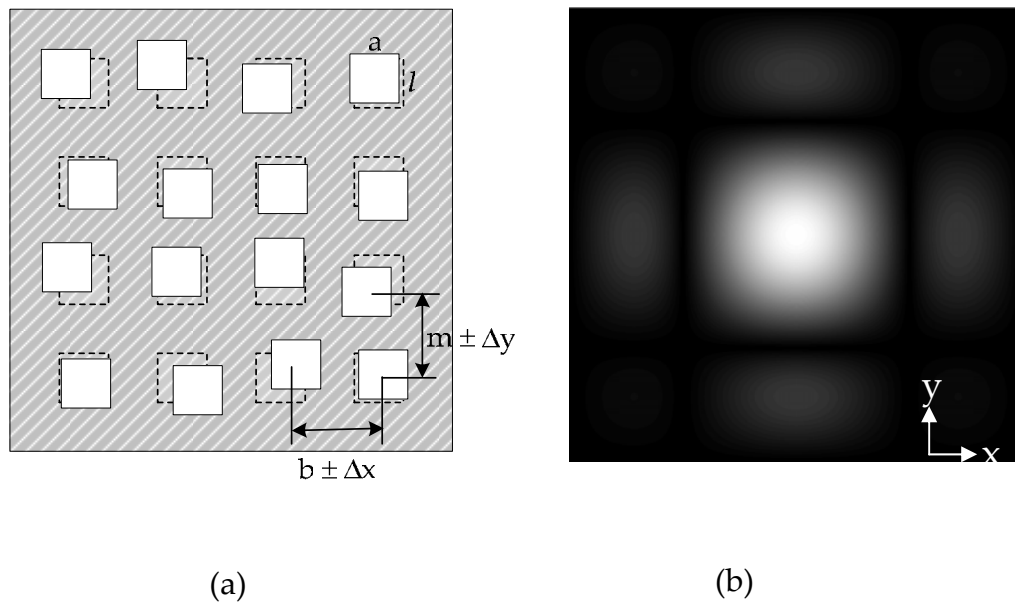
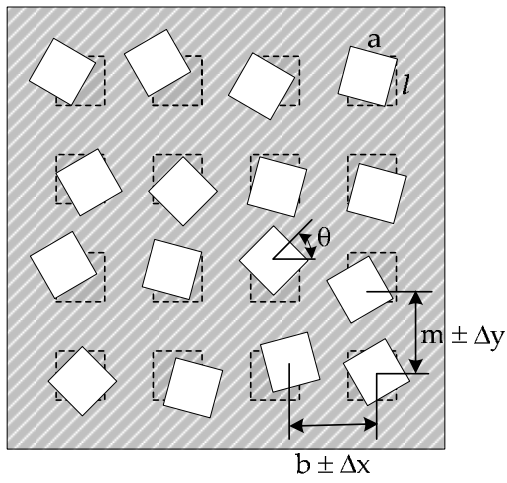
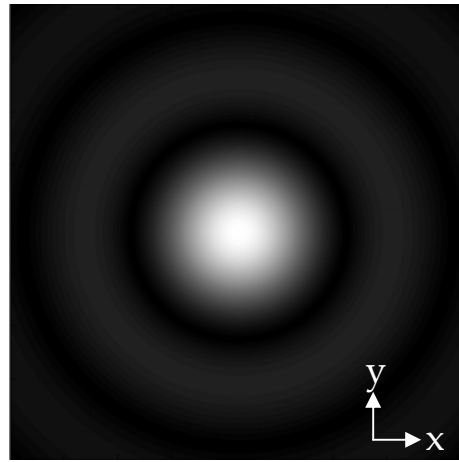


Fig. 4. (a) Geometric parameters of the translated etch holes layout, dash line represents the original position and solid lines represents the random offset by discrete uniform distribution (b) calculated irradiance pattern.



(a)



(b)

Fig. 5. (a) Geometric parameters of the random distributed etch holes layout, dash line represents the original position and solid lines represents the position after random translation and rotation (b) calculated irradiance pattern.

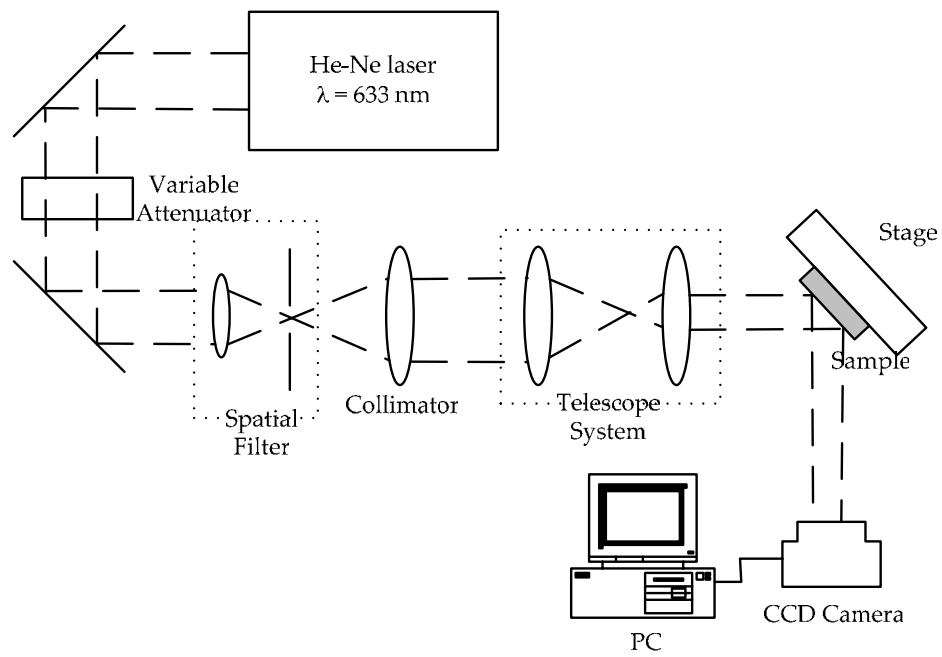
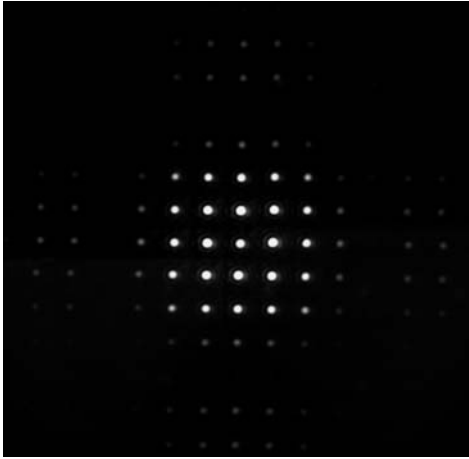
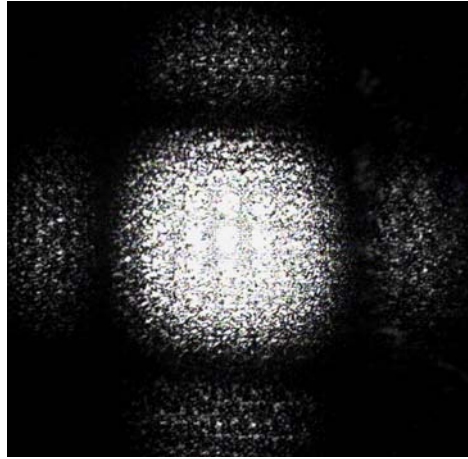


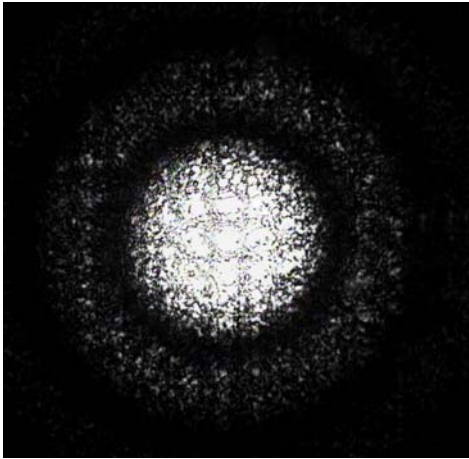
Fig. 6. Schematic configuration of the measurement system.



(a)



(b)



(c)

Fig. 7. The measured irradiance patterns of various etch-holes features (a) periodic square etch-holes array (b) etch-holes array with random translation (c) etch-holes array with random translation and rotation.

Optical properties of surface micromachining with randomly distributed etch holes

Chung-Hao Tien

Department of Photonics and Display Institute, National Chiao Tung University, Hsinchu, Taiwan,

30010

Tel:886-3-5131584, Fax: 886-3-5737681, Email: chtien@mail.nctu.edu.tw

Chi-Hung Lee

Department of Photonics and Institute of Electrical-Optical Engineering, National Chiao Tung

University, Hsinchu, Taiwan, 30010

Abstract Optical micromachining or microelectromechanical systems (MEMS) typically require etch holes to reduce the time required to release the micromechanical structure during the sacrificial undercutting. However, high-order diffraction beams caused by the periodic etch-holes array often deteriorate the optical performance by generating noise and erroneous crosstalk signals in most optical systems. In this paper, we studied the diffraction from a perforated micromirror and proposed a random distributed etch-holes layout. Due to the superposition of cosine functions with random periods, noise caused by high-order beams can be averaged out effectively.

Index Terms – MEMS, etch holes, diffraction

The micromachining, or microelectromechanical systems (MEMS) technology, which implements a functional system to be monolithically integrated on a single chip, has opened up many new possibilities for free space systems.¹⁻³ Compared with conventional macroscale devices, MEMS-based devices ranging in size from a few millimeters to a dozen microns provide smaller, lighter, faster and more rugged characteristics. In particular, optics is an ideal target since photon has no mass and is much easier to actuate than other macroscale objects. This advantage leads to a variety of optical elements such as binary-amplitude Fresnel zone plate for beam shaping,⁴ micromirror arrays for digital micromirror devices (DMD),⁵ and micropositioning stage for laser-to-fiber coupling,⁶ etc.

There is a number of MEMS micro fabrication technologies developed today, such as silicon bulk micromachining, LIGA, and surface micromachining.⁷ Silicon bulk micromachining uses chemical etchants sensitive to the orientation of the crystal lattice to remove the bulk region of the substrate and form a desired feature. LIGA process exposes a sheet of PMMA bonded to a wafer using X-ray lithography. After that, PMMA is then developed and the exposed material is removed. By Nickel electroplating and micromolding process, a high-aspect-ratio structure can be formed. Compared with previous two approaches, surface micromachining process, on which alternating layers of structural and sacrificial materials are deposited and patterned to create various structures by means of a VLSI (very large scaled integrated)-like process. Therefore,

many different devices can be fabricated on the same substrate using a standard foundry process. For this reason, surface micromachining process has become the most popular approach for MEMS fabrication. For surface micromachining process, the most well known recipe is to use polysilicon as the structural material and silicon oxide as the sacrificial material due to the excellent mechanical properties of polysilicon and high selectivity of sacrificial etching with hydrofluoric acid. As the sacrificial etching process is facilitated to release a large-area microstructure, it is common to distribute an etch-holes array over the microstructure to minimize the duration so that all undesirable etching of other films or structures shall be reduced.⁸ Fig. 1 shows a scanning electron microscopy (SEM) picture of a typical microplate with an etch-holes array. The periodic perforated pattern is represented in the inset, where a and b represents the element size and period of the square etch-holes array, respectively. Theoretically, the diffraction caused by such two-dimensional (2D) etch-holes array is analogous to the case in which a uniform plane wave is diffracted by a crossed grating. According to Fraunhofer diffraction theory,⁹ the diffracted irradiance $I(x,y)$ can be obtained by Fourier transform of the two-dimensional etch-holes array and thus be represented as

$$I(x, y) = \sum_{n=-N}^N \text{sinc}^2\left(\frac{a}{\lambda z} x\right) \text{sinc}^2\left(\frac{a}{\lambda z} y\right) \delta\left(\frac{b}{\lambda z} x - n\right) \delta\left(\frac{b}{\lambda z} y - n\right)$$

In this formula, the quadratic phase factor was suppressed, z and N represents the

propagation distance and number of etch holes, respectively. As the example, we consider a metal membrane perforated by an etch-holes array with square size $a = 5 \mu\text{m}$ and period of $b = 20 \mu\text{m}$ in both x and y directions, respectively. After illuminated by a collimated He-Ne laser ($\lambda = 0.63 \mu\text{m}$) under normal incidence, the transmitted irradiance of the diffracted beams in the far field can be observed, as shown in Fig. 2. The diffracted pattern consists of an array of bright spikes with the spacing $\Delta = \lambda z/b$. For this particular array, the ratio between the aperture width a and the period b is $b/a = 4$. Therefore, the fourth spikes overlaps with the first null of side lobe and the intensity of the fourth spike is disappeared. Although square-shaped etch holes frequently appear in the design, the actual shape of etch holes after plasma etching tends to be circular rather than square due to imperfect photolithography and etching process. In this case, the irradiance distribution caused by the square element is more like *Bessel* function rather than the *sinc* function in Eq. (1), as shown in the Fig. 2. The measured normalized intensity of the lowest few orders are 1 [0th order], 0.83 [(1,0), (0,1) order], 0.66 [(1,1) order], 0.45 [(2,0), (0,2) order], which are in a close agreement with theoretical values. Although small etch holes typically have little or no effect on the performance of electromechanical behavior,¹⁰ this is not the case for the optical function. From this study, we note that the presence of these periodic features can lead to considerable amount of high-order beams, which can potentially deteriorate optical performance by generating noise and erroneous crosstalk signals in most micro-optical systems. Although the magnitude of

the high-order beams can be suppressed by either decreasing the density of each-hole array or increasing the size of each aperture element, the expense of too small or large filling factor can result in poor optical properties and difficulty during the fabrication process.

According to the preceding study, how to eliminate the high-order diffracted beams without loss of fabrication convenience is needed. Fig. 3 shows the geometric parameters of the new photomask layout. We propose applying a random distributed etch-holes array, in which each square aperture in the x, y direction is translated by a random distance $(\Delta x, \Delta y)$ from its original position, where the translated distance $(\Delta x, \Delta y)$ are generated by the computer according to discrete uniform distribution.¹¹ In addition, one more requirement on the spacing between each etch holes should be considered to avoid the possibility of fabrication failure. When the spacing is too far, the etchant is hard to reach the center of the large-area micromechanical structure. On the contrary, when the spacing is too close, the mechanical strength of perforated surface is weakened and the polysilicon thin film is easily broken while film is lifted out of the wafer. Therefore, we add a condition that the distance between each element shall be within the range of $20 \pm 5 \mu\text{m}$ in this case. Besides the translation, we also randomize each aperture element with respect to rotation angle θ between $[-\pi/4, \pi/4]$ as well to alleviate the shape factor effect of each aperture element. Detailed design and considerations are in preparation for another publication.

Experiments on randomly distributed holes-array were carried out. Fig. 4 shows the irradiance image of the light passing through a randomized perforated micromirror in comparison with the simulation results. In this configuration, the diffraction pattern looks like one obtained by rotating a single etch hole diffraction pattern about its center, which suggests the interference terms caused by the periodicity was cancelled by the superposition of cosine functions with random periods introduced via translation design (Δx , Δy). In addition, the diffraction pattern of the square aperture is average out via random rotation angle as well.

In summary, we have investigated the effects of etch-holes array on the optical properties of micromachined structures with $\lambda = 0.63 \mu\text{m}$. As long as two conditions are met (1) the etch holes must large compared with the wavelength, and (2) the diffracted fields must not observed too close to the aperture, our analysis in this paper can be applied to different wavelengths by scaling all the geometric parameters involved proportionally. According to our study, etch-holes array exerts two major effects on the diffraction pattern, namely, array factor and shape factor. The array factor determined by the period of the etch holes can cause high-order diffraction beams, which can be averaged out by means of random translation distribution. On the other hand, shape factor determined by the form of the each hole provides the envelope of the overall diffraction pattern, which can be alleviated by randomly rotating each element of the array. Optical experiments quantitatively confirmed the proposed design of random

distributed etch-holes array. Such etch-holes layout is expected to alleviate the noise caused by high-order diffracted beams and improve the optical performance in most optical-MEMS devices.

This work was supported by the National Science Council, the Republic of China under contract no. NSC 94-2215-E-009-028. C. H. Tien's email address is chtien@mail.nctu.edu.tw.

References

1. M. C. Wu, "Micromachining for optical and optoelectronic systems" *Proc. IEEE*, Vol. 85, pp. 1833-1856, 1997.
2. W. S. Trimmer, *Micromechanics and MEMS-Classic and Seminar Papers to 1990*. Piscataway, NJ: IEEE Press, 1997.
3. K. E. Petersen, "Silicon as a mechanical material," *Proc. IEEE*, Vol. 70, pp. 420-457, 1982.
4. L. Y. Lin, S. S. Lee, K. S. J. Pister, and M. C. Wu, "Three-dimensional micro-Fresnel optical elements fabricated by micromachining techniques," *Electron. Lett.*, Vol. 30, no. 17, pp.448-449, 1994.
5. P. F. V. Kessel, L. J. Hornbeck, R. E. Meier, and A. R. Douglass, "A MEMS-based projection display" *Proc. IEEE*, Vol. 86, pp. 1687-1704, 1998.
6. M. J. Daneman, O. Solgaard, N. C. Tien, K. Y. Lau, and R. S. Muller, "Laser-to-fiber coupling module using a micromachined alignment mirror," *IEEE Photon. Technol. Lett.*, Vol. 8, pp. 396-398, 1996.
7. J. Bryzek, K. Petersen and W. McCulley, "Micromachines on the march," *IEEE Spectrum*, Vol. 31, no. 5, pp.20-31, 1994.
8. J. Zou, M. Balberg, C. Byrne, C. Liu and D. J. Brady, "Optical properties of surface

micromachined mirrors with etch holes," *IEEE J. Microelectromech. Syst.*, Vol. 8, no. 4, pp. 506-513, 1999.

9. M. Born and E. Wolf, *Principle of Optics*, New York: Pergamon Press, 1980.
10. T. Veijola and T. Mattila, "Modeling of nonlinear micromechanical resonators and their simulation with harmonic-balanced method" *Proc. Transducers'01, Germany*, pp. 1506-1509, 2001.
11. W. H. Beyer, *CRC Standard Mathematical Tables, 28th ed.*, Florida: CRC Press, 1987.

Figure captions

Fig. 1. SEM of a microplate with an etch-holes array. The periodic perforated pattern is represented in the inset, where a and b represents the element size and period of the square etch-holes array, respectively.

Fig. 2. (a) Measurement (b) Simulated irradiance distribution of the diffracted beams of a metal membrane perforated by periodic an etch-holes array with square size $a = 5 \mu\text{m}$ and a period of $b = 20 \mu\text{m}$ in both x and y directions, respectively.

Fig. 3. Geometric parameters of the random distributed etch-holes layout. Dash line represents the original periodic position and solid line represents the position after random process.

Fig. 4. (a) Measurement (b) Simulated irradiance distribution of the randomly distributed holes-array.

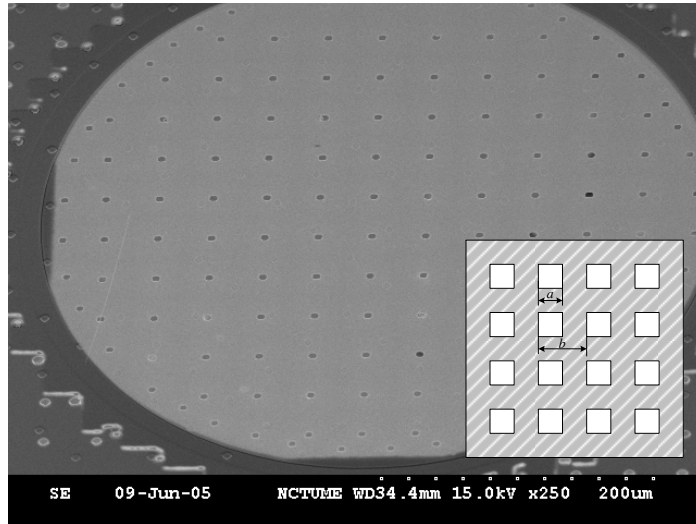
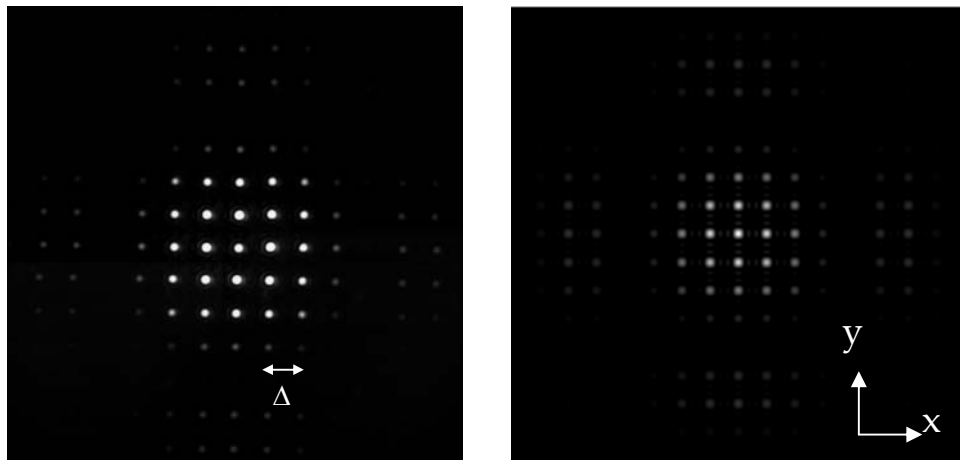


Fig. 1. SEM of a microplate with an etch-holes array. The periodic perforated pattern is represented in the inset, where a and b represents the element size and period of the square etch-holes array, respectively.



(a)

(b)

Fig. 2. (a) Measurement (b) Simulated irradiance distribution of the diffracted beams of a metal membrane perforated by periodic an etch-holes array with square size $a = 5 \mu\text{m}$ and a period of $b = 20 \mu\text{m}$ in both x and y directions, respectively.

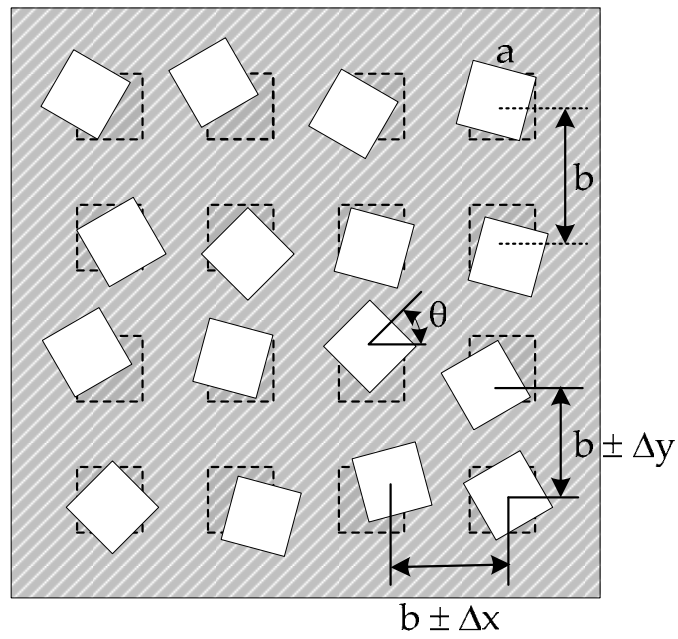
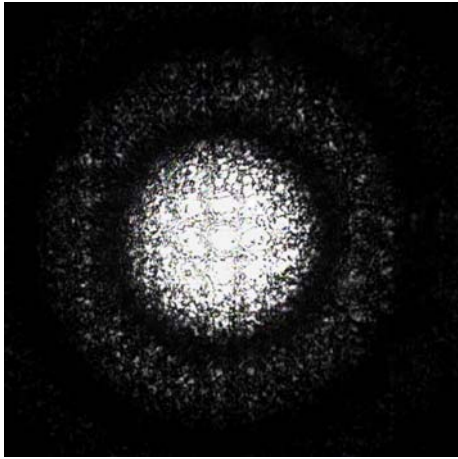
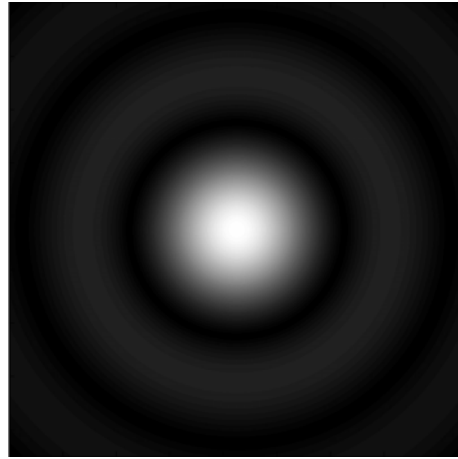


Fig. 3. Geometric parameters of the random distributed etch-holes layout. Dash line represents the original periodic position and solid line represents the position after random process.



(a)



(b)

Fig. 4. (a) Measurement (b) Simulated irradiance distribution of the randomly distributed holes-array.